Palaeogeography, Palaeoclimatology, Palaeoecology 560 (2020) 109971

Contents lists available at ScienceDirect

Palaeogeography, Palaeoclimatology, Palaeoecology

journal homepage: www.elsevier.com/locate/palaeo

Cenozoic cooling history and fluvial terrace development of the western domain of the Eastern Kunlun Range, northern Tibet

Chen Wu[a,*], Jie Li[b], Andrew V. Zuza[c], Changfeng Liu[d], Wencan Liu[d], Xuanhua Chen[e], Tian Jiang[f], Bing Li[c,e]

[a] Key laboratory of Continental Collision and Plateau Uplift, Institute of Tibetan Plateau Research, Center for Excellence in Tibetan Plateau Earth Sciences, Chinese Academy of Sciences, Beijing 100101, China
[b] School of Earth Sciences and Resources, China University of Geosciences (Beijing), Beijing 100083, China
[c] Nevada Bureau of Mines and Geology, University of Nevada, Reno, Nevada 8957, USA
[d] Institute of Geological Survey, China University of Geosciences (Beijing), Beijing 100083, China
[e] Chinese Academy of Geological Sciences and China Geological Survey, Beijing 100037, China
[f] School of Ocean Sciences, China University of Geosciences (Beijing), Beijing 100083, China

ARTICLE INFO

Keywords:
Tibetan plateau
Thermochronometry
OSL dating
Apatite fission track
Shortening rate

ABSTRACT

The growth of the Tibetan Plateau resulted primarily from Cenozoic India-Asia collision and continued convergence, and thus the deformation timing and geomorphic evolution of northern Tibet are critical to understanding the dynamics of orogenic plateau growth. Although previous studies have suggested that the Altyn Tagh Shan and the Eastern Kunlun Range of northern Tibet have experienced differential faulting and exhumation history, our knowledge of the temporal and spatial distribution of the growth of the northwestern Tibetan Plateau is still lacking. In this study, we integrate new geologic mapping, low-temperature themochronometry (18 apatite-fission track ages), and Optically Stimulated Luminescence (OSL) dating to provide constraints on the Cenozoic cooling history of northwestern Tibet and late Quaternary fluvial terrace development. We focus on where Altyn Tagh Shan structures are juxtaposed against Eastern Kunlun Range structures. New fission-track cooling ages from one traverse along the Aksu River yielded three cooling age domains: Paleocene, Miocene, and early Pliocene. With this new knowledge of ~12–10 Ma initiation of Jianxiashan thrusting and exhumation, we suggest a refined N-S shortening rate of this thrust system of 2.0–2.4 mm/yr and strain rates of 8–9 $\times 10^{-16}$ s^{-1}. Thermal history modeling suggests that the study area experienced two broad events, including slow cooling through the AFT PAZ since the early Eocene and rapid cooling during the late Miocene. Our OSL dating results from the Aksu drainage reflect two separate processes of aggradation and incision that occurred during the late Pleistocene and Holocene, respectively, which are interpreted to result from long-term forcing of incision by a constant rate of tectonic uplift modulated by late Quaternary climatic variations. We interpret that this incision occurred at a rate of ~1 mm/yr, which is faster than exhumation rates inferred from the AFT data (0.3–0.5 mm/yr). These Quaternary exhumation rates may reflect faster recent exhumation or uplift associated with the proximal Altyn Tagh fault. In accordance with previous studies, we present a refined Cenozoic tectonic model for the evolution history of northern Tibet. The deformation pattern of northern Tibet results from clockwise rotation of preexisting weaknesses and transpressional deformation along the Kunlun fault and the Haiyuan fault.

1. Introduction

Crustal thickening and uplift during orogenic plateau development impacts hazards, natural resources, and climate (e.g., Bilham et al., 2001; Molnar et al., 2010; Brooks et al., 2011; Richards, 2011). The growth of the Tibetan Plateau in the Himalayan-Tibetan orogen provides insights into this dynamic continental tectonics process and allows us to better understand other past and present orogens (e.g., Molnar, 1988; Taylor and Yin, 2009; Yin, 2010; Clark, 2012; Garzione et al., 2017; Zuza et al., 2020). To decipher this plateau growth requires refined knowledge of the temporal–spatial distribution of Cenozoic continental deformation in northern Tibet (e.g., Meyer et al., 1998;

* Corresponding author.
E-mail addresses: wuchen@itpcas.ac.cn (C. Wu), azuza@unr.edu (A.V. Zuza), liuchangfeng@cugb.edu.cn (C. Liu), liuwenc@cugb.edu.cn (W. Liu), xhchen@cags.ac.cn (X. Chen), jiangtian@cugb.edu.cn (T. Jiang), libing@cags.ac.cn (B. Li).

https://doi.org/10.1016/j.palaeo.2020.109971
Received 12 June 2020; Received in revised form 23 July 2020; Accepted 5 August 2020
Available online 29 August 2020
0031-0182/

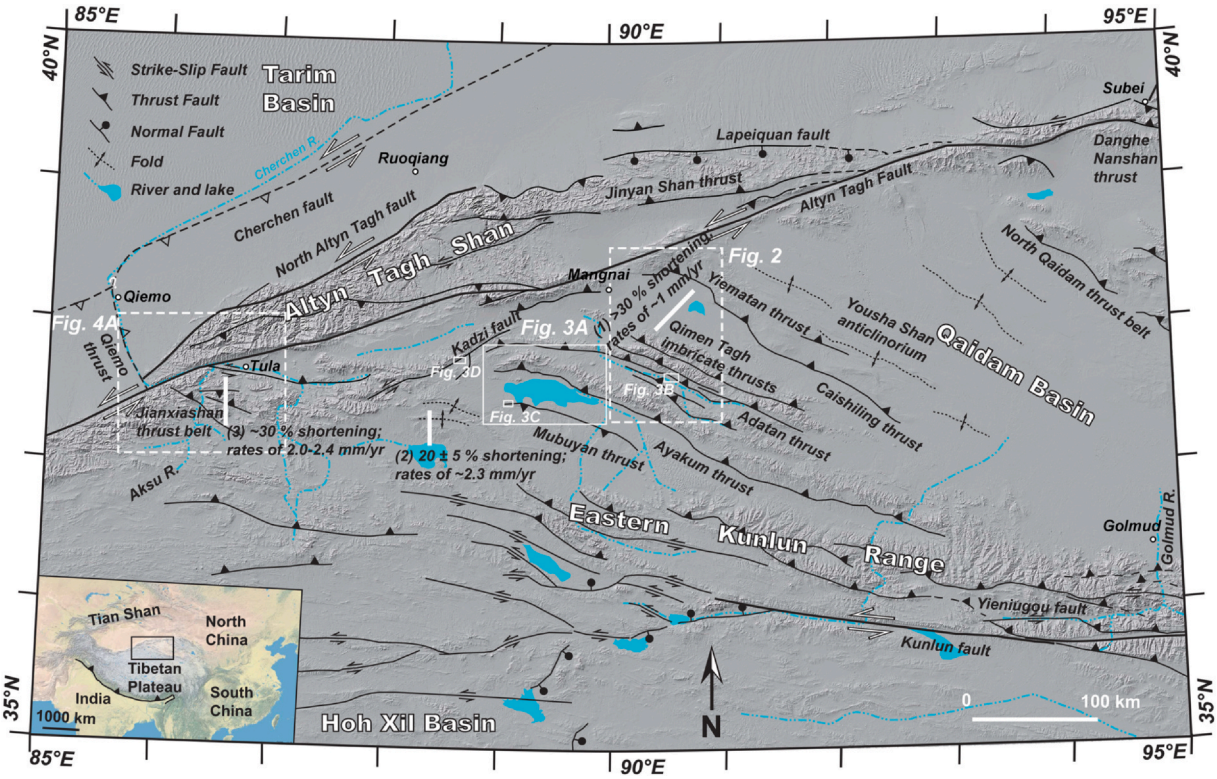

Fig. 1. Regional tectonic map of the northwestern Tibetan Plateau from Yin and Harrison (2000), Taylor and Yin (2009), Yin et al. (2007, 2008a), Wu et al. (2019a, 2020). Underlying base map is from GeoMapApp software, available online at www.geomapapp.org (Ryan et al., 2009). The shortening estimates sources are: (1) Yin et al. (2007); (2) Yakovlev (2015); (3) Wu et al. (2020). The inset shows the location of Himalayan-Tibetan orogen, and the black box exhibits the regional tectonic map area.

Jolivet et al., 2001; Clark et al., 2010). The most prominent Cenozoic geological features in northern Tibet include the Eastern Kunlun transpressional system, the Qilian Shan fold-thrust belt, and the left-lateral strike-slip Haiyuan fault system, and the Altyn Tagh fault system (e.g., Burchfiel et al., 1989; Meyer et al., 1998; Zuza and Yin, 2016; Wu et al., 2019a; Tapponnier and Molnar, 1977; Yin, 2010). Previous research suggests that northern Tibet experienced deformation shortly after the India-Asia collision (e.g., Yin and Harrison, 2000; Dupont-Nivet et al., 2004; Clark et al., 2010; Duvall et al., 2011) and has undergone accelerated deformation since the Miocene (e.g., Meyer et al., 1998; Molnar and Stock, 2009).

The mechanism and timing for the uplift of northern Tibet remains poorly constrained, especially in the west at the junction of the Qilian Shan, the Altyn Tagh and the Kunlun Ranges (Fig. 1). Existing thermochronometry studies suggest that ca. 50–45 Ma deformation was distributed across much of northern Tibet, and deformation has most recently accelerated since the Miocene (e.g., Jolivet et al., 2001; Dupont-Nivet et al., 2004; Horton et al., 2004; Yin et al., 2008a, 2008b; Clark et al., 2010; Duvall et al., 2011, 2013; Yuan et al., 2013; Qi et al., 2016; He et al., 2018; Li et al., 2019, 2020). A series of active thrust faults link the Kunlun fault and Altyn Tagh fault systems and are responsible for the Cenozoic uplift of the Eastern Kunlun Range, the Qimen Tagh, and the Qilian Shan (Figs. 1 and 2). The initiation of uplift of the Eastern Kunlun Range may have started locally in the early Cenozoic (e.g., Clark et al., 2010; Duvall et al., 2011, 2013), but the majority of uplift started with the initiation of the Kunlun left-slip fault at ca. 20–16 Ma, which is contemporaneous with the initiation of Haiyuan left-slip fault system to the north (e.g., Yin et al., 2008a; McRivette et al., 2019; Wu et al., 2019b; Jolivet et al., 2001; Craddock et al., 2011; Duvall et al., 2013; Yuan et al., 2013; Zuza and Yin, 2016; Li et al., 2019). Earlier studies have suggested that rapid exhumation of the Altyn Tagh Shan region occurred either at 26 Ma (Sobel et al., 2001), 18–15 Ma (Wang et al., 2006; Ritts et al., 2008), or 10–7 Ma (Jolivet et al., 1999, 2001). Regardless of the exact timing, it is suggested that the exhumation resulted mainly from slip on the North Altyn Tagh fault rather than on the present main strand of the Altyn Tagh fault (e.g., Cowgill et al., 2000; Ritts et al., 2008; Sobel et al., 2001; Shi et al., 2018).

Two general end-member models have been proposed for deformation and uplift of northern Tibet: (1) out-of-sequence deformation where northern Tibet initiates earlier (i.e., Eocene), and deformation jumps back to the Eastern Kunlun in the Miocene (e.g., Jolivet et al., 2001; Dupont-Nivet et al., 2004; Horton et al., 2004; Yin et al., 2008a, 2008b; Clark et al., 2010; Duvall et al., 2011, 2013; Yuan et al., 2013; Qi et al., 2016; He et al., 2018; Li et al., 2019; Zuza et al., 2019; Wu et al., 2019a, 2019b), and (2) in-sequence northeast-propagation models where deformation systematically migrated to the northeast, matched by northeastward growth of the plateau (e.g., Meyer et al., 1998; Tapponnier et al., 2001; Liu-Zeng et al., 2008; Zheng et al., 2010, 2017; Yu et al., 2019a, 2019b). Models within this latter group suggest that earlier northeastward progression (Yin et al., 2007; Wang et al., 2003) occurred in the Eocene-Oligocene, whereas other groups suggest that Miocene deformation reached the northeasternmost plateau (e.g., Yue and Liou, 1999; Sun et al., 2005; Wang et al., 2020; Zheng et al., 2017; Pang et al., 2019). Across the Jianxiashan thrust belt in this region, Wu et al. (2020) determined an average geologic shortening rate of 1.2–0.9 mm/yr, based on bedrock geologic mapping, and structural and stratigraphic constraints (Fig. 1), assuming deformation initiated at ca. 25–20 Ma. However, this initiation age was not well constrained. Therefore, we sought to determine deformation initiation ages across this thrust system to provide deformation ages in this understudied region and refine our previously estimated shortening rates across the Jianxiashan thrust belt (Fig. 1).

Drainage patterns are sensitive to the uplift process, and fluvial

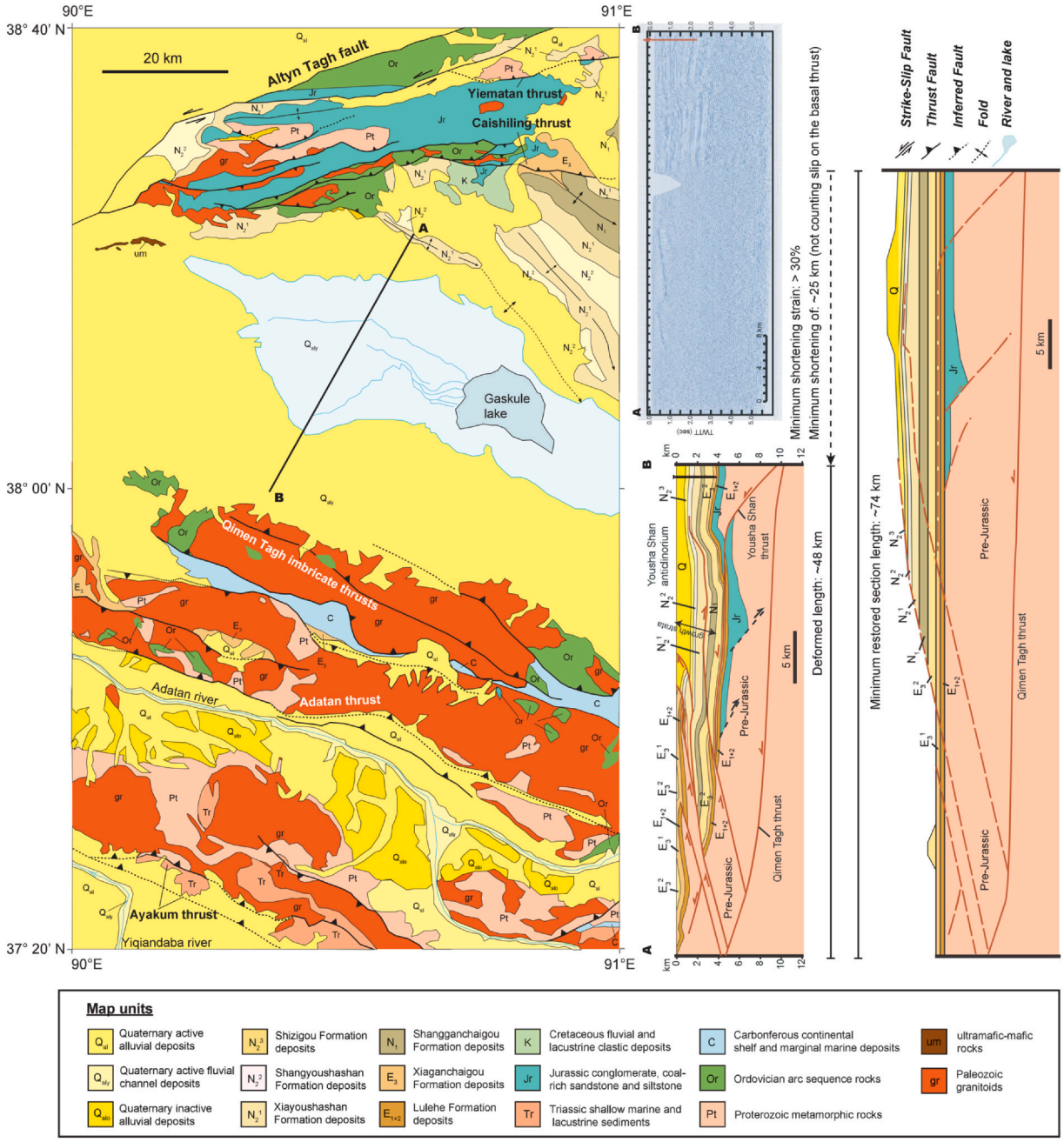

Fig. 2. Geologic map of the Qimen Tagh and southwestern Qaidam region from Yin et al. (2007), see Fig. 1 for location. The seismic profiles A-B and balanced cross section are modified from Yin et al. (2007) and Chen et al. (2010).

terraces can be used to quantitatively assess the active deformation (e.g., Seeber and Gornitz, 1983; Kirby and Whipple, 2001; Van der Woerd et al., 2002; Owen et al., 2006). During the Cenozoic uplift of northern Tibet, incision of several north-flowing drainages entering Qaidam Basin from the Eastern Kunlun Range have produced extensive fluvial terrace sequences that show no obvious evidence of significant tectonic activity along the range front (e.g., Wang et al., 2009; Chen et al., 2011b, 2011a; Kapp et al., 2011; Yu et al., 2020). However, less attention has been focused on the small, north-flowing Aksu drainage in the western end of the Eastern Kunlun Range (Wu et al., 2020), which drains into the Cherchen river across the Altyn Tagh left slip fault, the Qiemo thrust, and the Cherchen left slip fault (Fig. 1). Analysis of the Quaternary terrace development can be related to uplift and incision to derive deformation rates (e.g., Cowgill, 2007; Zhang et al., 2018). Whether these vertical uplift rates are related to strike-slip deformation or thrust-belt development is enigmatic. In addition, whether tectonic uplift rates have remained constant throughout the late Cenozoic is unknown, which requires comparison of ~10-Myr-timescale uplift rates with Quaternary rates.

In this study, we document the structural and thermochronological cooling history of the northwestern Tibetan Plateau. We present field observations and satellite image interpretations, and apatite fission-track (AFT) low-temperature thermochronometry data. AFT samples were collected along the Aksu river from a duplex thrust structural traverse and from within the Altyn Tagh fault system. Our results shed light on thrust and strike-slip fault-related exhumation and activity. In addition, we combined field observations and optical stimulated luminescence (OSL) dating of multiple levels of fluvial terraces preserved along the Aksu drainage to quantify late Quaternary spatial and temporal incision rates related to uplift and shortening in northwestern

Tibet. Our interdependent goals were to (1) provide new constraints on Cenozoic cooling history of the western domain of the Eastern Kunlun Range, (2) compare and analyze Cenozoic shortening rates with late Quaternary fluvial terrace development of the western domain of the Eastern Kunlun Range, and (3) improve our understanding of the Cenozoic tectonic evolution of the northern Tibet.

2. Regional geology

2.1. Cenozoic Altyn Tagh Shan

The Altyn Tagh tectonic boundary involves oblique kinematics, including strike-slip faulting, fold-thrust belts, and fault-bounded basins (e.g., Che et al., 1995; Cowgill et al., 2000; Yin and Harrison, 2000; Chen et al., 2003) (Fig. 1). The ~1600-km long left-slip Altyn Tagh fault is one of the largest strike-slip faults in the Indo-Asian collisional zone, which defines the northwestern boundary of the Tibetan Plateau. The Altyn Tagh fault experienced multiple pulses of Cenozoic activity (e.g., Che et al., 1995; Cowgill et al., 2000; Yin and Harrison, 2000; Chen et al., 2003) and possibly a pre-Cenozoic history (e.g., Yue and Liou, 1999) (Fig. 1). Estimates of the cumulative displacement along the left-slip fault are ~400 km (e.g., Yang and Li, 2006; Yin and Harrison, 2000; Ritts and Biffi, 2000; Yin et al., 2002; Cowgill et al., 2003; Chen et al., 2003; Cheng et al., 2015). The active Altyn Tagh fault started developing at ca. 49 Ma, and the kinematically linked Jinyan Shan and Danghe Nanshan thrust faults formed at ~50–40 Ma in the Altyn Tagh and Nanshan regions (e.g., Yin et al., 2002) (Fig. 1). The Altyn Tagh fault accommodates relatively discrete strain during progressive displacement between the Qaidam and Tarim blocks. Strain along this fault consists of strike-parallel simple shear and fault-normal contractional deformation, which further controlled the formation and evolution of the Cenozoic Qaidam Basin (e.g., Chen et al., 2010; Wu et al., 2019a). Furthermore, the western margin of the Qaidam Basin developed as an open synclinorium (e.g., Yin et al., 2007; Chen et al., 2010). The present geometry of the left-slip Altyn Tagh fault in the Altyn Tagh Shan developed at ~30–20 Ma, evidenced by the fault cutting the Jinyan Shan and Danghe Nanshan thrust faults (e.g., Yin et al., 2002; Chen et al., 2003, 2010) (Fig. 1).

The inferred Cherchen fault is parallel to and northwest of the Altyn Tagh fault (Fig. 1). Previous research has suggested the fault is left-slip, despite a lack of reliable field and satellite imagery evidence (e.g., Xinjiang Bureau of Geology and Mineral Resources (BGMR), 1993, 2003) (Fig. 1). The NNW-striking Qiemo thrust separates the eastern and western segments of the Cherchen fault along the Cherchen river. The thrust is not obvious in the field (Fig. 1), however, the fault juxtaposes areas of different geology and the antecedent streams at east of the Qiemo thrust are merged into the Cherchen river (e.g., Xinjiang Bureau of Geology and Mineral Resources (BGMR), 1993, 2003; Wu et al., 2020) (Fig. 1).

2.2. Cenozoic western domain of the Eastern Kunlun Range

The Kunlun fault system is interpreted to have initiated by reactivation of a pre-existing early Mesozoic suture in response to broad north-south right-slip shear and/or clockwise rotation of northern Tibet (Zuza and Yin, 2016; Wu et al., 2016, 2019a). Age constraints of deformation indicate that the fault system has been coevally active since at least the late Miocene and the clockwise rotation has occurred since the Neogene (e.g., Yin et al., 2007, 2008a). The western part of Eastern Kunlun Range is dominated by the westward-widening, triangular-shaped Qimen Tagh thrust belt. This thrust belt merges with the Kunlun fault and Yousha Shan anticlinorium (Yin et al., 2007, 2008a) (Fig. 1). Individual thrusts in the Qimen Tagh thrust belt are dominantly south- and southwest-directed and link locally with minor east- and northeast-trending left-slip faults (Figs. 1 and 2). If the thrust faults have comparable displacements along strike, the westward widening of the thrust belt may imply a corresponding increase in crustal shortening magnitude to the west. Previous work along the northern margin of Eastern Kunlun Range suggests that the region is dominated by south-directed thrusts (Yin et al., 2007) and related intermontane basins with deposition beginning in the Oligocene (Zhong et al., 2004; Xia et al., 2020). The existence of a major south-dipping, range-bounding thrust fault has been inferred (e.g., Burchfiel et al., 1989; Chen et al., 1999; Mock et al., 1999; Yin and Harrison, 2000; Jolivet et al., 2001), with seismological evidence in the southwest Qaidam Basin cited to support this south-directed thrust geometry (e.g., Chen et al., 1999) (Fig. 2). Such activity, primarily associated with north-dipping thrust faults, suggests that the range is experiencing ongoing uplift.

However, this model has been challenged by the reinterpretation of the seismic reflection profiles by Yin et al. (2007), who suggest the existence of a minor north-directed backthrust in the hanging-wall of a deeper north-dipping, south-directed thrust. Field relationships further confirm this reinterpretation, including the daylighting of this south-directed fault within the Eastern Kunlun Range (Yin et al., 2007; Chen et al., 2010). The reinterpreted seismic reflection profile across western Qaidam Basin, shown in Fig. 2, records the development of Jurassic half-grabens in the north, and north-south Cenozoic shortening strain (Fig. 2). Well-developed Quaternary growth strata suggest that deformation is active and shortening initiated in the Oligocene time (Fig. 2), which implies an average mid-Cenozoic to present shortening rate of ~1 mm/yr or strain rates of ~4.3×10^{-16} s^{-1} (e.g., Yin et al., 2007, 2008a; Chen et al., 2010) (Figs. 1 and 2).

Nearly all major thrusts within the western domain of the Eastern Kunlun Range, north of the left-slip Kunlun fault, are south-directed (Fig. 2). Some of the thrusts are linked with east-striking left-slip faults that are sub-parallel to the Kunlun fault or terminate at northeast-striking left-slip faults associated with the Altyn Tagh fault system. Structures here include the Yiematan and Caishiling thrusts south of Yousha Shan anticlinorium (Yin et al., 2007) (Fig. 2), and Qimen Tagh imbricate thrusts south of Gaskule syncline (Fig. 2). The Adatan river makes a sharp turn northward and flows into Qaidam Basin across the trace of the active Adatan thrust (Fig. 2). To the east, the Adatan thrust can be traced over a low divide at the headwaters of the Adatan River and into the southern Qaidam Basin beyond where decreasing slip is likely accommodated by minor deformation within the Cenozoic basin strata (Fig. 3A). Recent tectonic activity on the western segment of the Adatan thrust is indicated by a series of discontinuous low fault scarps that are preserved across alluvial fan surfaces (Fig. 3B). The Ayakum thrust can be traced along the northern margin of the large and roughly triangular-shaped Ayakum basin, which is cut by multiple fault branches. The northern strands place Paleozoic granite and lower Paleozoic strata over Mesozoic sediments, and the southern strands juxtapose Paleozoic granite and strata against Cenozoic strata (e.g., Pan et al., 2004; Yin et al., 2007) (Figs. 2 and 3A). Similar to the Adatan thrust, the Ayakum thrust trace exhibits a curved geometry and likely terminates at structures related to left-slip along the Altyn Tagh fault system at its western end or links with a north-directed Cenozoic thrust zone to the south of the Tula basin (e.g., Robinson et al., 2003; Dupont-Nivet et al., 2004) (Fig. 3A).

To south of the active Ayakum thrust, active surface uplift and folding is evident in satellite imagery (Fig. 3A). This uplifted area is bounded to the north by the north-directed Mubuyan thrust (Wu et al., 2020), which extends from the folds at the western end of the basin that obscures the eastern continuation of the fault trace (Fig. 3C). The Kadzi fault bends to the west towards the Altyn Tagh fault and may link with structures in the Tula uplift region (e.g., Robinson et al., 2003; Wu et al., 2020) (Fig. 1). The Kadzi fault also appears to accommodate displacement on the Adatan and Ayakum thrust systems, which both terminate near the mapped trace of the Kadzi fault. The Kadzi fault offsets geomorphic features such as drainage channels in a possible left-lateral sense (Fig. 3D). Yakovlev (2015) reported ~9-km of shortening (20 ± 5% strain) across a 36-km-long traverse of the Guaizi Liang

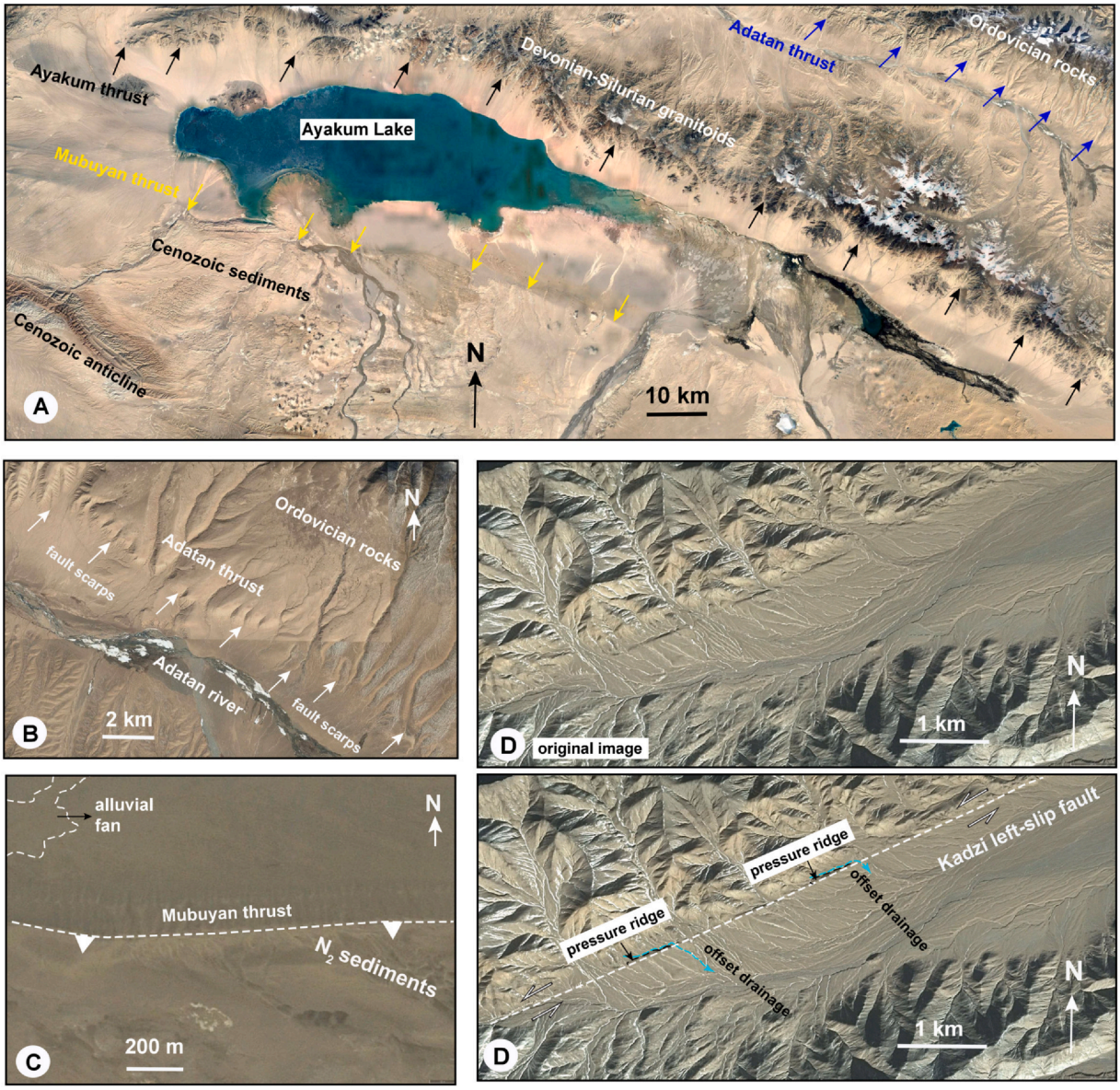

Fig. 3. Satellite image interpretations of thrusts in the western domain of the Eastern Kunlun Range, the base images are from Google Earth. The locations are shown in the Fig. 1.

within the Kumkuli basin near the Mubuyan thrust (Fig. 1). Uplifted Quaternary alluvial fan surfaces suggest that deformation is active. The combination of the cross section reconstruction of Yakovlev (2015) and dating of this uplifted surface yielded a Pleistocene-to-present shortening rate of 1.7 ± 0.5 mm/yr. Based on their interpreted shortening initiation age of 5.3–2.6 Ma, Yakovlev (2015) suggested a Pliocene-to-present shortening rate 2.3 ± 0.9 mm/yr.

3. Geology of Qiemo area

Our study area is located at the junction between the Altyn Tagh and the Eastern Kunlun Range along the Cherchen river and Aksu river, close to Qiemo city (Figs. 1 and 4A). Precambrian sedimentary strata were deposited along the northwestern margin of the Qiemo area along the Cherchen river, and are intruded by Late Neoproterozoic and early Paleozoic granitoids (e.g., Xinjiang Bureau of Geology and Mineral Resources (BGMR), 1993, 2003; Wu et al., 2020) (Fig. 4A). Late Neoproterozoic, Early Paleozoic, and Late Paleozoic-Early Mesozoic arc magmatism were associated with the development of Kunlun oceans and the South Altyn Tagh ocean (e.g., C.L. Wu et al., 2014; Liu et al., 2015; Kang et al., 2016; Wu et al., 2020) (Fig. 4A). Lower Carboniferous shallow marine strata are exposed as a thrust klippe on top of Upper Jurassic sedimentary (Wu et al., 2020), and there is a widespread unconformity represented by Jurassic strata overlying Proterozoic basement (e.g., Xinjiang Bureau of Geology and Mineral Resources (BGMR), 1993, 2003; Wu et al., 2020). Scattered Lower Cretaceous to Cenozoic continental strata overlie highly folded Jurassic strata across the Qiemo area (Fig. 4A). In this study, we constructed a balanced cross section and kinematic restoration for the region just south of the Cherchen river, where deformation is predominately dip-slip, and Carboniferous–Cretaceous bedded strata provided geometric information (Fig. 4B).

Our previous geochronology results indicated that the plutons of the study area crystallized between ~446 and ~ 331 Ma (i.e., Jianxiashan pluton, Fig. 4A) (Xinjiang Bureau of Geology and Mineral Resources (BGMR), 1993, 2003; Wu et al., 2020; Jiao et al., 2020). Minor early Mesozoic granitoid dikes were also mapped intruding the migmatite in the Qiemo area (Xinjiang Bureau of Geology and Mineral Resources (BGMR), 1993, 2003; Wu et al., 2020). Late Paleozoic–early Mesozoic granitoids and dikes are scattered across the study area (Xinjiang BGMR, 1993, 2003; Wu et al., 2020). The Jianxiashan pluton covers an

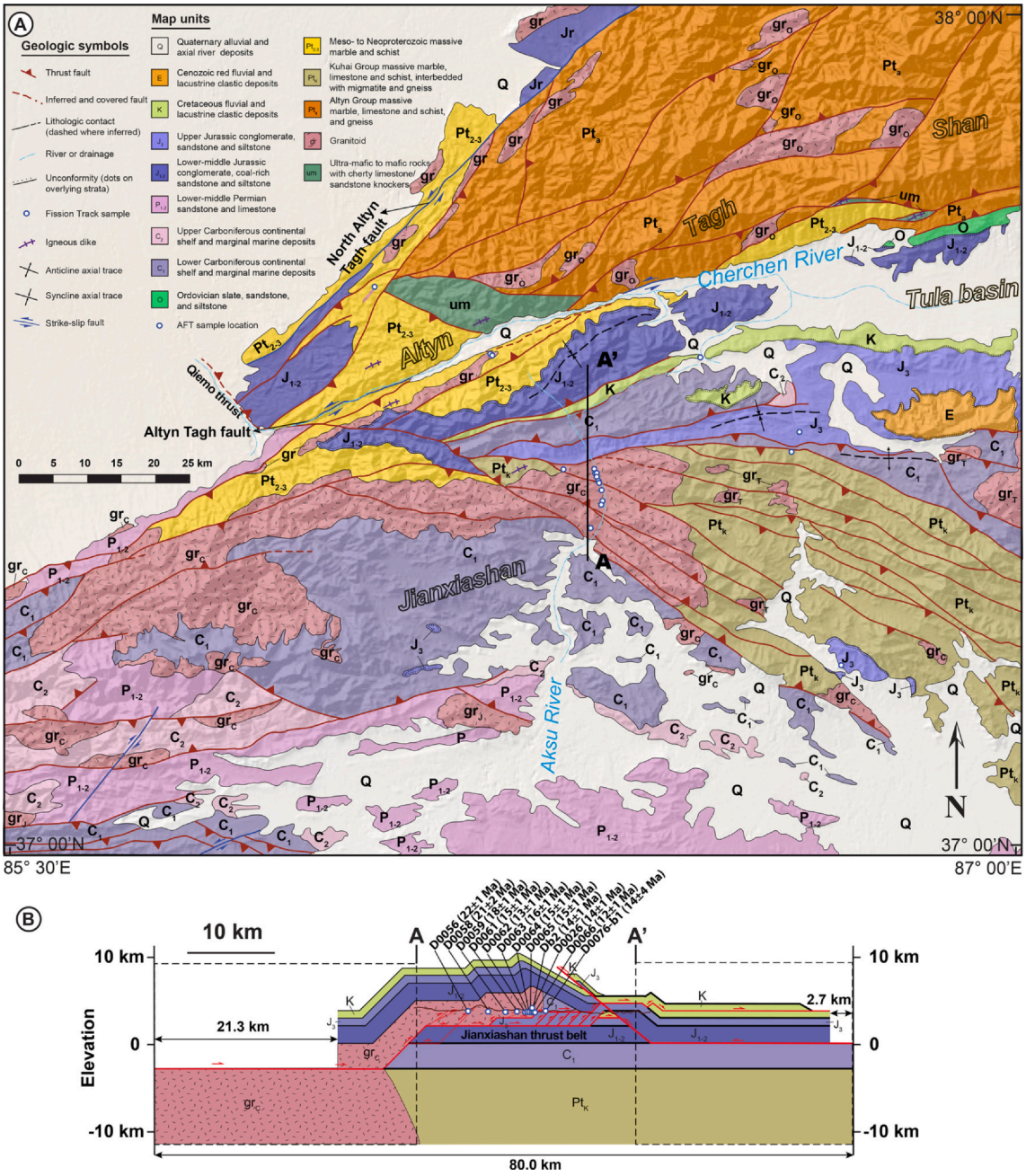

Fig. 4. (A) Regional geologic map of the western domain of the Eastern Kunlun Range based on a compilation of Xinjiang Bureau of Geology and Mineral Resources (BGMR) (1993, 2003) and the geologic mapping and structural interpretations from Wu et al. (2020); see Fig. 1 for location. (B) Cross-section A–A′ shows the shortening magnitudes and Jianxiashan AFT sample locations, where the brown line is the topographic line, and the dashed boxes are the possible interpretation for the extension of the section A–A′. (For interpretation of the references to colour in this figure legend, the reader is referred to the web version of this article.)

area of ~1000 km^2 and is composed of granodiorite (Fig. 5A and B), diorite (Fig. 5C), and granite (Fig. 5D). There is minor sub-solidus deformation (Fig. 5B) in the central and north domains, medium-grained tonalite (Fig. 5E) in the core, and medium- to fine-grained two-mica monzogranites along the south margin (Fig. 5F).

Tectonically, the Qiemo area is dominated by the Jianxiashan thrust belt, which consists of a collection of mostly north- and northeast-dipping thrusts that are responsible for uplift of the range. The dip-slip thrust belt is oriented obliquely to, and possibly merges with, the Altyn Tagh fault in the west. Restoration of a ~ 56-km-long balanced cross section across this thrust belt revealed minimum Cenozoic shortening of ~24 km (~30% strain) (Fig. 4B) (Wu et al., 2020). This study did not have precise constraints on the initiation age of this deformation, and conservatively assumed that shortening commenced after ca. 25–20 Ma based on regional interpretations of the deformation age for the Qimen Tagh thrust belt (e.g., Jolivet et al., 2001, Jolivet et al., 2003; Yin et al., 2007, 2008a, 2008b). With this age estimate, we previously estimated that the thrust belt experienced shortening at a rate of 1.2–0.9 mm/yr^{-1} and strain rates of 4.7 × 10^{-16} s^{-1} to 2.3 × 10^{-16} s^{-1}, which overlaped with established Cenozoic and present-day strain rates across much of the Himalayan-Tibetan orogen (e.g., Clark, 2012; Zuza et al., 2018, 2019; Haproff et al., 2019; Wu et al., 2020). The relatively slow rates of contractional deformation were used to infer that crustal shortening did not significantly contribute to left-slip offset on the Altyn Tagh fault, which has must faster slip rates of ~10 mm/yr (e.g., Cowgill et al., 2009).

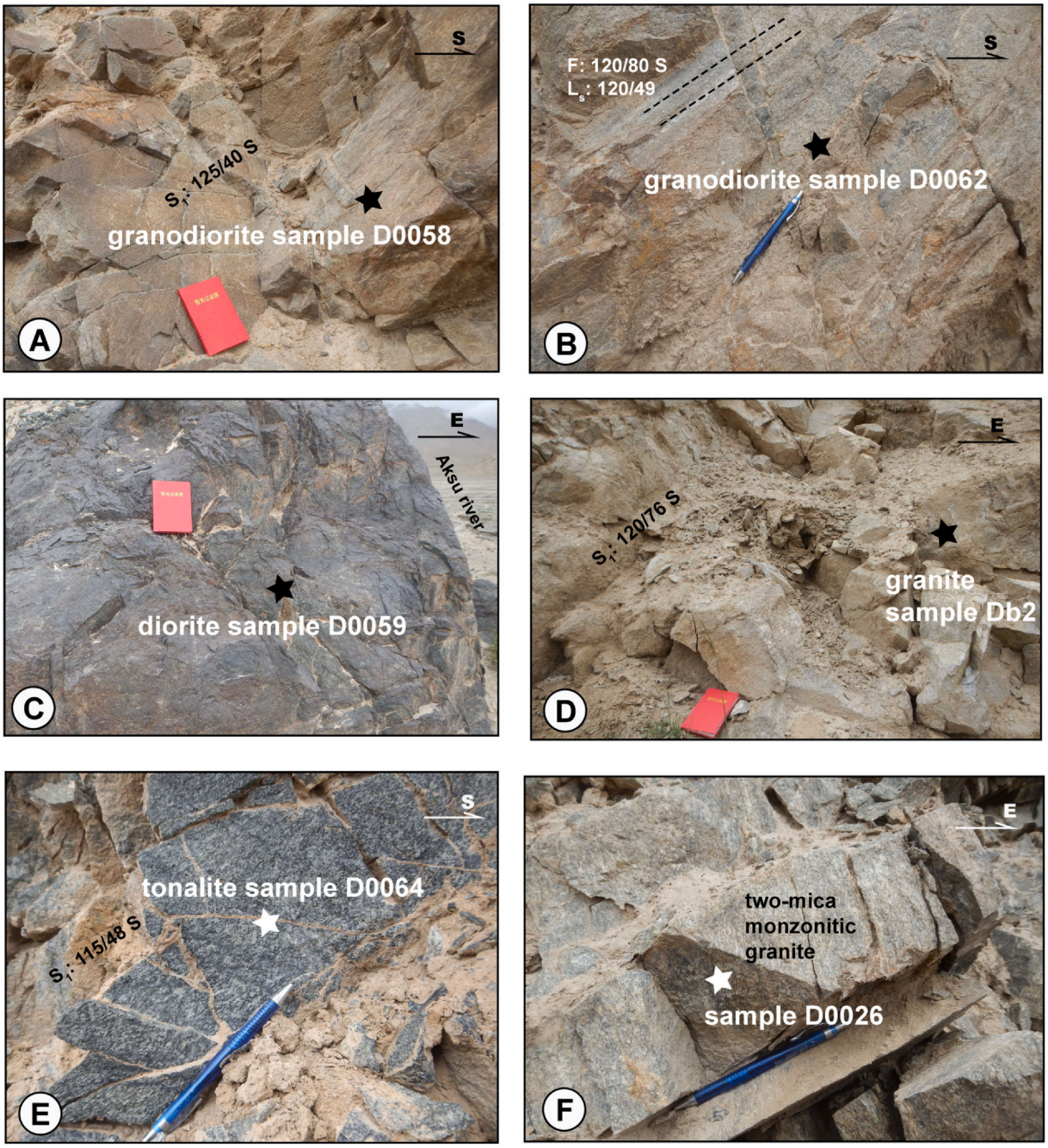

Fig. 5. Field photos of the Jianxiashan pluton and show the representative apatite fission-track samples.

4. Fluvial terraces along the Aksu drainage

The Aksu river drainage flows northward from the Kunlun Range and drains into the Cherchen river located along the southeastern margin of the Altyn Tagh Shan (Fig. 6). The Cherchen river flows southwestward in the study area where terraces exhibit high elevation (Figs. 6A and 7A). Fluvial incision along the Aksu drainage has produced an impressive sequence of inset terraces downstream to the north (Fig. 6A and C). Northward from a prominent bedrock inselberg near the range front (Fig. 6B), three main terrace surfaces (T_1–T_3) are recognized above the modern channel (T_0) Aksu drainage (Fig. 6C and D). Each main terrace T_1 through T_3 consists of a suite of surfaces that exhibit minor elevation differences relative to the main surface (Fig. 7B, C, and D).

The surveyed Aksu drainage terraces can be divided into two reaches. The downstream reach extends northeast from the meander bend to the toe of the terraces and trends ~N40°E (Fig. 6A). The upstream reach trends ~N10°E from the range front to a tight bend adjacent to a prominent bedrock inselberg (Fig. 6B). Topographic maps, satellite images, and field observations demonstrate serval important features of the Aksu terraces: (1) upstream terraces are rather poorly developed (Fig. 7E), whereas downstream terraces have a gentle concavity and converge towards the Cherchen river in the north and the Tula basin in the east (Fig. 6A and C); (2) terrace surfaces show no obvious evidence for structural deformation resulting from surface faulting or folding (Figs. 6C, 7B and D); and (3) numerous terrace surfaces are preserved over relatively short spatial extents (Fig. 7B and C).

T_3 might be a minor fill terrace that is formed by valley aggradation and subsequent channel incision into the alluvium, and only exists on

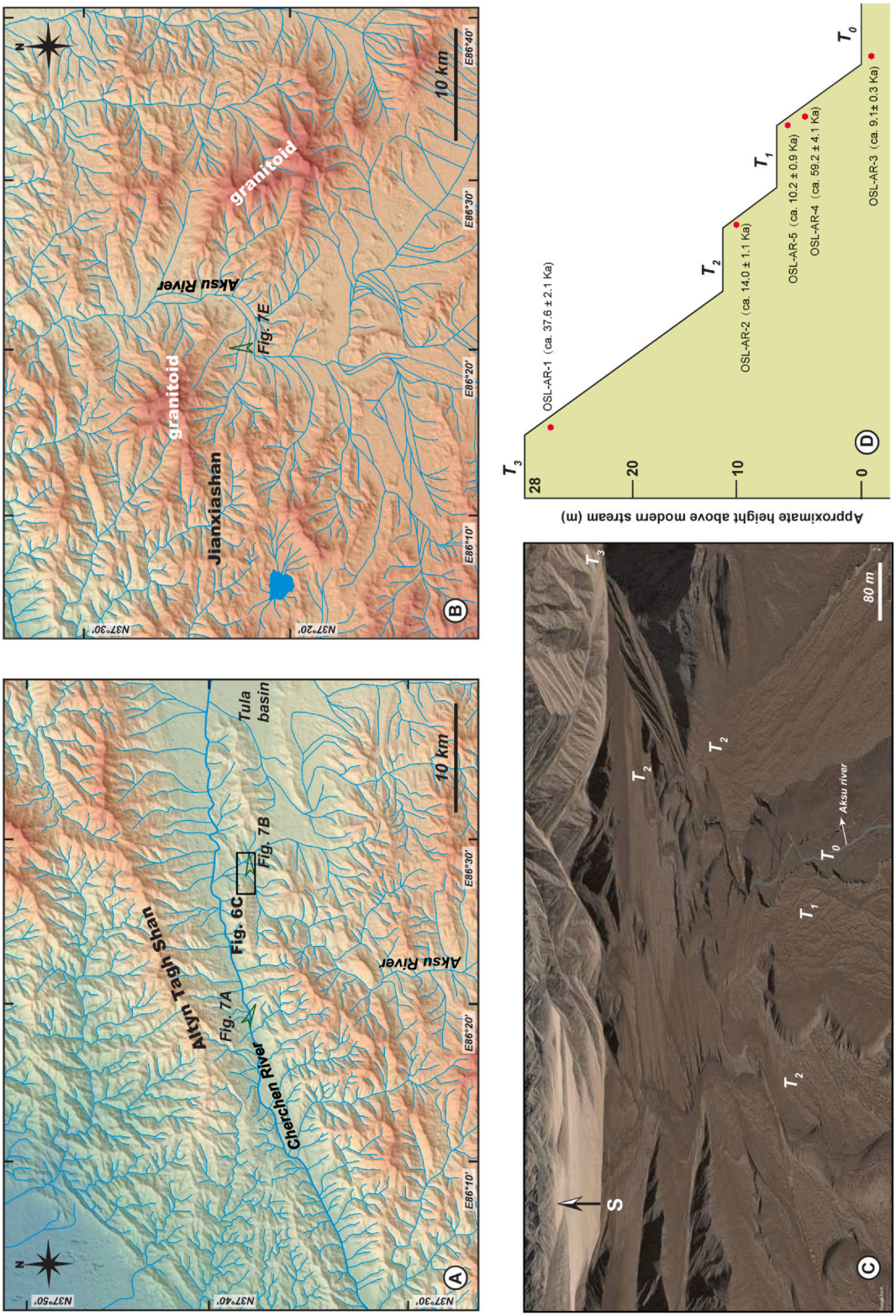

Fig. 6. DEM images with 30-m resolution for the Aksu and Cherchen rivers. (A) The Aksu drainage flows northward into the Cherchen river and the Tula basin, and the downstream reach extends northeast from the meander bend to the toe of the terraces and trends ~N40°E; (B) The upstream reach trends ~N10°E from the range front proper to a tight meander bend adjacent to a prominent bedrock inselberg; (C) Google Earth image showing the distribution of fluvial terraces along the Aksu river; (D) Schematic cross-section of the geomorphologic surfaces along Aksu drainage. OSL sample locations are shown in their morphostratigraphic positions along with analytical results.

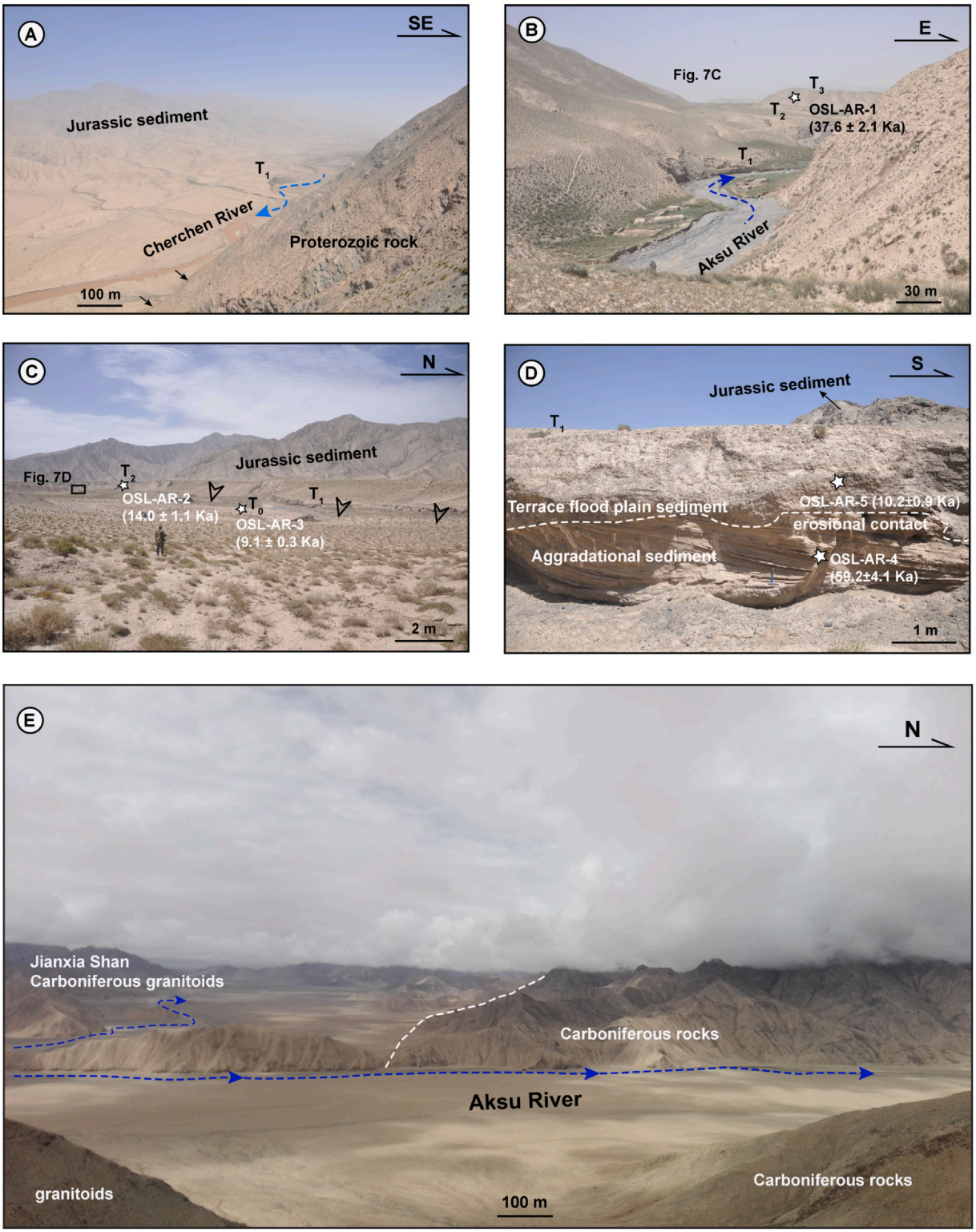

Fig. 7. Field photos of the Cherchen and Aksu drainage terraces and locations of OSL samples in this study.

the east side of the active channel (Figs. 6D and 7B). T_2 and T_1 exist on the both sides of active channel, but T_1 on the east side of active channel is mostly eroded because it has been displaced to the active channel and eroded by stream flow (Figs. 6C and 7D). T_0 is the active floodplain (Fig. 7B and C). Its deposits are weakly cemented by carbonate in the upstream area and consist of gravel bar and abandoned braided channel deposits in the downstream region (Fig. 7C and E).

5. Fission-track thermochronology

Fission-track thermochronology is based on crystal-lattice damage manifested as linear tracks resulting from the constant-rate spontaneous fission of trace levels of ^{238}U in zircon and apatite grains. Fission tracks in apatite are incompletely annealed over the temperature range of 60–110/120 °C, which is termed the partial annealing zone (PAZ) (e.g., Gleadow, 1981; Gleadow et al., 2002; Ketcham et al., 2007). The

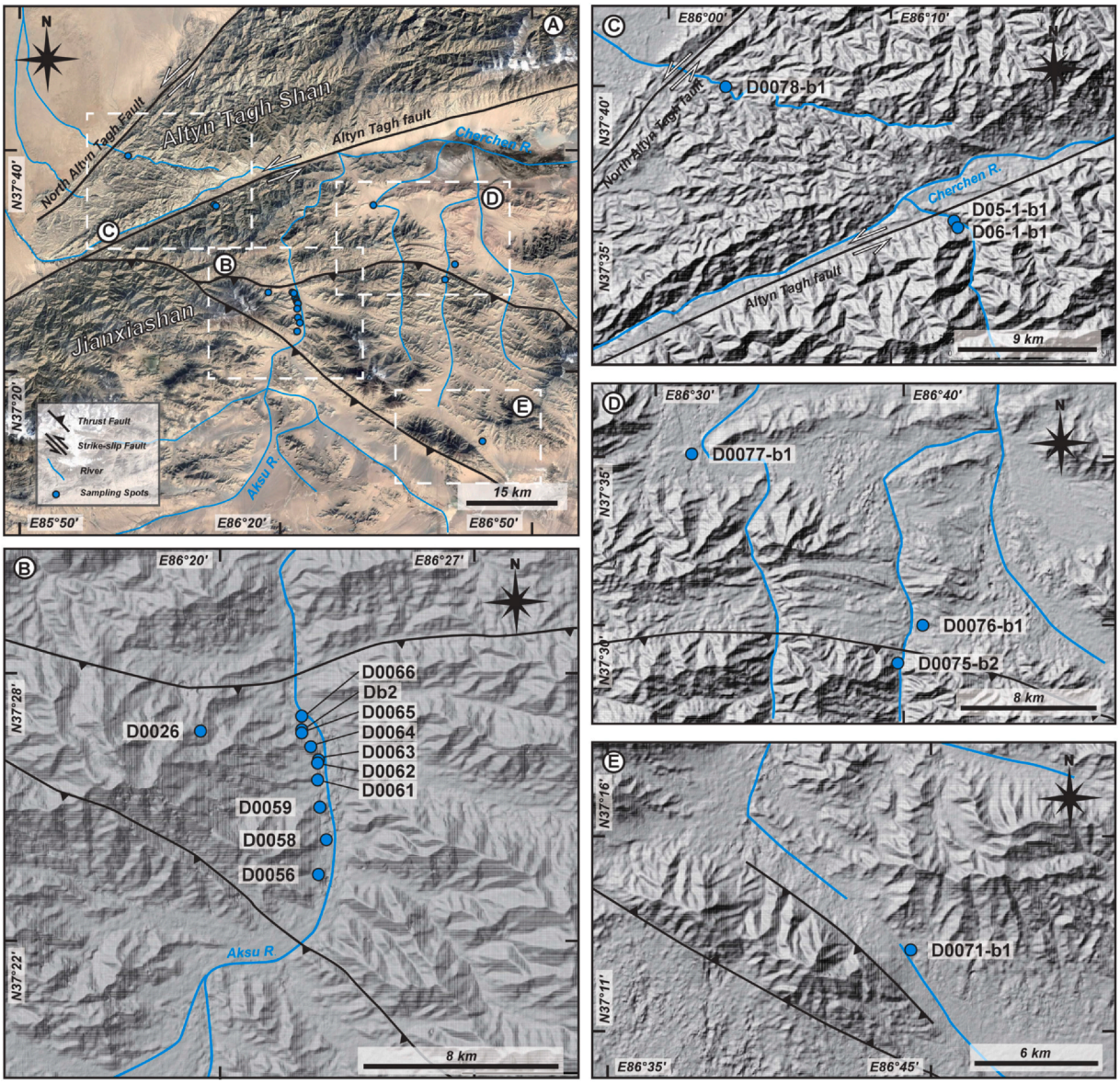

Fig. 8. Satellite image of the western domain of the Eastern Kunlun Range, (A) showing sample locations of the apatite fission-track samples, including (B) the Jianxiashan pluton, (C) Early Paleozoic granitoids near the North Altyn Tagh fault and Altyn Tagh fault, (D) the Jurassic and Cretaceous sandstones, and dike intruding the Proterozoic metamorphic rocks, and (E) Lower Carboniferous sandstone.

decrease in temperature of a sample through the partial annealing zone as a function of time is reflected by the distribution of lengths for the partially annealed tracks. We conducted Apatite Fission-Track (AFT) analyses on 18 samples to determine the low-temperature thermal history of the western end of the Eastern Kunlun Range along the Aksu river (Fig. 8).

Fission-track ages were measured using the external detector method (Gleadow, 1981) and calculated using the zeta calibration method with a Zeta value of 322.1 ± 3.6 (1 s) (Hurford and Green, 1983; Hurford, 1990). Apatite and zircon grains were separated from ~5-kg materials for each sample using standard mineral separation techniques. Polished grain mounts were prepared and etched to reveal spontaneous fission tracks. Apatite grain mounts were etched in 6.6% HNO_3 at 25 °C for 30 s, and all samples were irradiated at the China Institute of Atomic Energy reactor facility, Beijing. Low-U muscovite external detectors covering apatite grain mounts were etched in 40% hydrofluoric acid at 25 °C for 20 min to reveal induced fission tracks. In order to increase the number of observable horizontal confined tracks, the samples were exposed to ^{252}Cf (Donelick and Miller, 1991). Horizontal confined fission-track lengths (e.g., Laslett et al., 1987; Gleadow et al., 1986) were measured only in prismatic apatite crystals because of the anisotropy of fission track annealing in apatite (Green et al., 1986).

We collected fifteen Paleozoic granitoid and three sandstone samples for AFT analyses along the Aksu river. Sample locations and AFT pooled ages are shown on Fig. 8 and Supplement Table S1. Five AFT samples (D0056, D0063, D0076-b1, D0077-b1, and D0059) failed the χ^2 test (P (χ^2) < 5%; Galbraith, 1990) and have an age-dispersion over or equal to 15% (Fig. 9; Supplement Table S1; Vermeesch, 2009), indicating that more than one age component is present in the obtained single grain age population. For samples that passed the χ^2 test, the pooled ages are reported as AFT ages; otherwise, the central ages are adopted (Sobel et al., 2006). In addition, all AFT ages are much younger than crystallization and depositional ages (Wu et al., 2020), and we interpret them to represent cooling ages that may record regional exhumation events. AFT ages for almost all analyzed samples range between 22 ± 1 Ma and 4.7 ± 1 Ma (1σ), with the exception of the southernmost Carboniferous sandstone sample D0071-b1, which has a

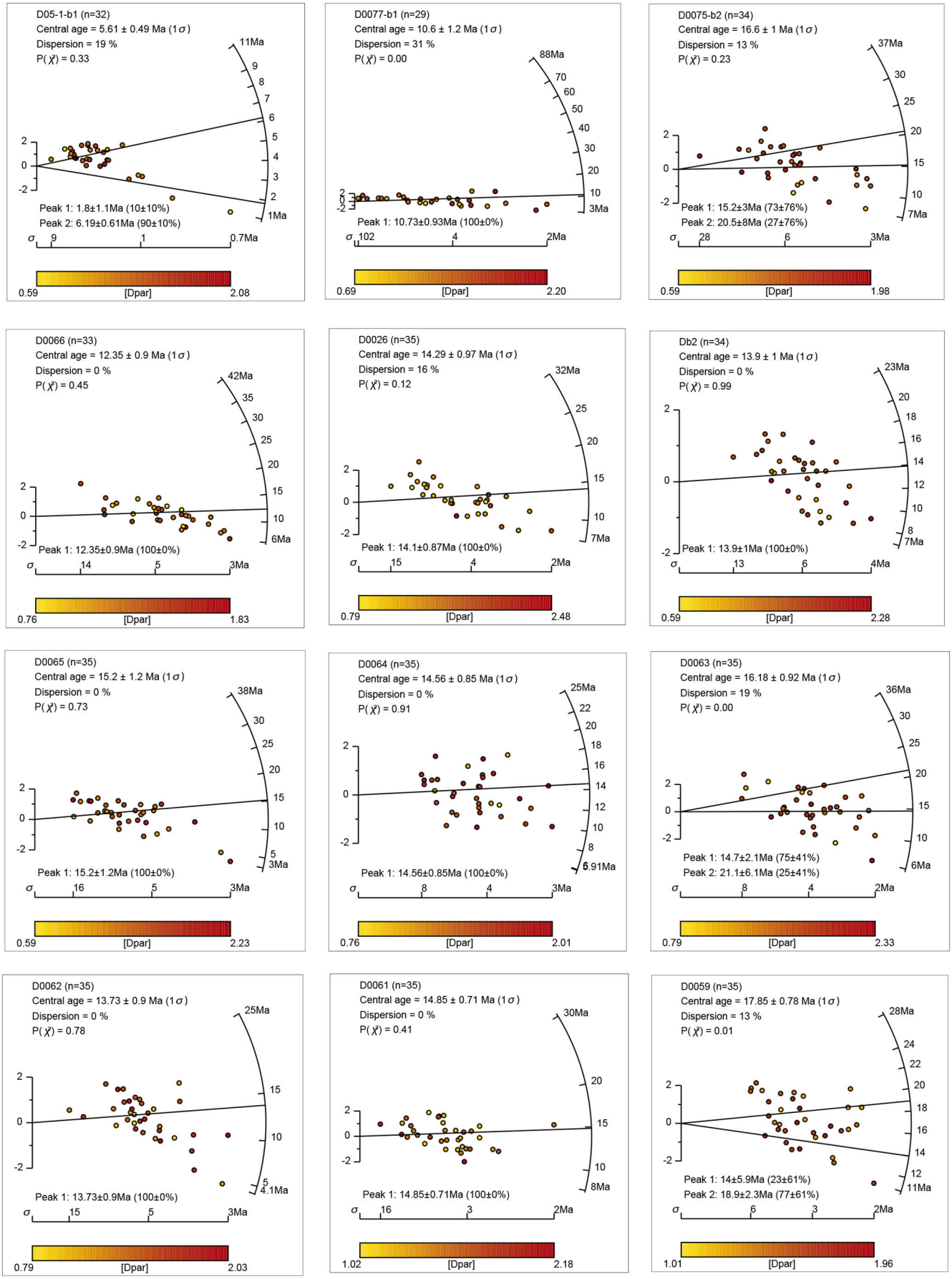

Fig. 9. Apatite fission-track radial plots from RadialPlotter by Vermeesch, 2009 of the study samples.

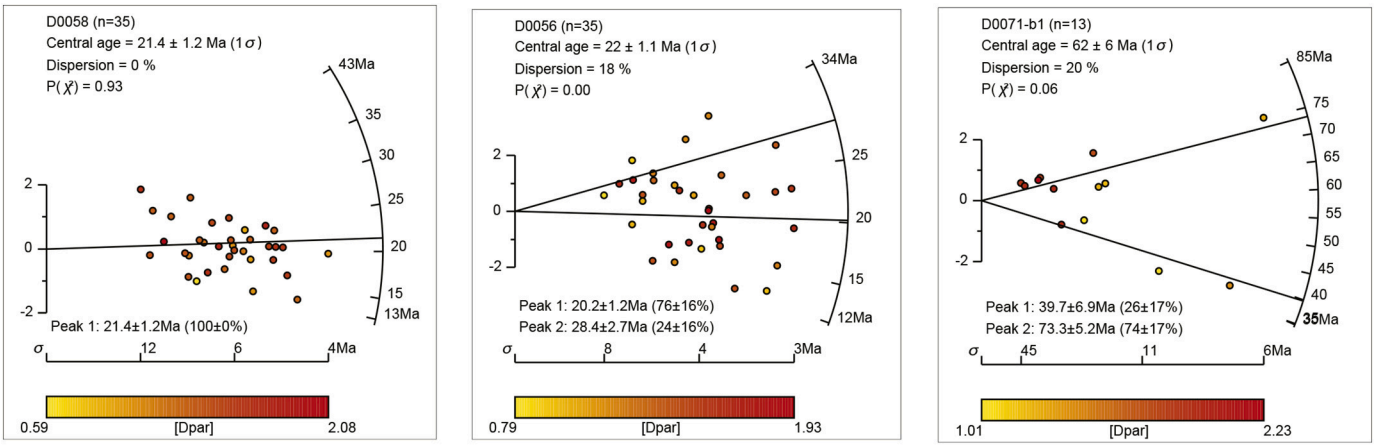

Fig. 9. (*continued*)

significantly older AFT age of 65 ± 5 Ma (1σ). Mean track lengths range between 11.8 ± 2.4 μm and 14.0 ± 0.1 μm. The AFT ages for samples of the Jianxiashan pluton along the Aksu river (Fig. 8B) increase generally southward, with the exception of samples D0062 and D0061 (Supplement Table S1). The northmost sample D0078-b1 was collected from an Early Paleozoic granite dike intruding the Mesoproterozoic metamorphic rocks within the Altyn Tagh Shan (Fig. 8C) and has an AFT age of 8.7 ± 1 Ma.

6. Thermal history modeling

Because fission track systematics in apatite are characterized by a PAZ between 60 and 110/120 °C, AFT ages and measured fission track length distributions can be inverted to produce suites of compatible thermal histories (e.g., Ketcham, 2005; Ketcham et al., 2007). We performed inverse modeling of the AFT data using the HeFTy v1.9.1 software of Ketcham (2005) and the kinetic annealing model for apatite of Ketcham et al. (2007). Samples were collected along a tributary of the Aksu River, but most were not collected along a single elevation profile (Fig. 8). Therefore, we modeled the AFT data for each sample separately (Fig. 10). Four samples were not modeled because they were either missing mean track length data (samples D0078-b1, D06-1-b1, and D0076-b1) or did not yield any satisfactory models (sample D0059).

Modeling of sample D05-1-b1 suggests cooling since the Late Miocene from a temperature above the upper limit of the AFT PAZ (~120 °C) and residence in the PAZ until the latest rapid cooling episode through the lower limit of the PAZ (~60 °C) since the Pliocene (Fig. 10). Samples D0077-b1 and D0075-b2 indicate steady cooling from a temperature above the upper limit of the PAZ since the Eocene and resided in the PAZ until it was cooled rapidly through the lower limit of the PAZ since the Late Miocene (Fig. 10). Almost all Late Devonian-Early Carboniferous Jianxiashan pluton samples (D0066, D0026, D0065, D0064, D0063, D0062, D0061, D0058, D0056) cooled from a temperature above the upper limit of the PAZ in the Paleocene-Early Eocene, and resided in the PAZ until it was cooled rapidly through the lower limit of the PAZ since the Late Miocene (Fig. 10). Sample Db2 with one exception exhibits cooling paths featured by initial rapid cooling in the Early-middle Miocene and residence in the PAZ until the latest rapid cooling episode through the lower limit of the PAZ since the Late Miocene (Fig. 10). The Lower Carboniferous sandstone sample D0071-b1 shows a thermal history with rapid cooling to the upper limit of the PAZ during the Late Cretaceous followed by residence in the PAZ until rapid cooling through the lower limit of the PAZ since the Middle Eocene (Fig. 10). We further use the thermal history modeling with good paths to discuss the cooling history of the western domain of the Eastern Kunlun Range (Fig. 11A).

7. Optical Stimulated Luminescence (OSL) dating at Aksu drainage

Samples for OSL dating were collected from terrace deposits along the Aksu river. Samples were collected by inserting steel tubes with 5 cm inner diameter and 20 cm length into terrace deposits under the sheltered condition. All samples were wrapped with silver paper and fixed with tape to prevent light and keep their water content. OSL age determination was performed at the Institute of Hydrogeology and Environmental Geology, Chinese Academy of Geological Sciences.

Samples were pretreated with 30% HCl and 40% H_2O_2 to remove the carbonates and organic material, respectively, and then immersed in H_2SiF_6 (30%) for 3 days to obtain the quartz component. All measurements were performed using maximum power in a Daybreak2200 automated OSL reader equipped with a combined blue (470 ± 5 nm, maximum power 60 mW/cm^2) and infrared (880 ± 80 nm, maximum power 80 mW/cm^2) LED OSL units, and a $^{90}Sr/^{90}Y$ beta sources (0.103871 Gy/s) for irradiations (e.g., Rhodes, 2011). The sensitivity-corrected multiple-aliquot regenerative-dose protocol (SMAR) was applied for most of our samples to yield one value of equivalent dose (De) for each sample (e.g., Rhodes, 2011). This protocol uses multiple aliquots of fine-grained quartz grains (8–15 μm) to build the growth curve, and it corrects the sensitivity changes with a test dose to each aliquot. Neutron Activation Analysis (NAA) was used to measure the uranium, thorium, and potassium concentrations for all samples.

In this study, a total of five sediment samples were collected from geomorphic surfaces along the downstream reach at Aksu drainage for OSL dating (Fig. 6D). Fluvial sand samples from terraces T_1 (samples OSL-AR-4 and OSL-AR-5), T_2 (samples OSL-AR-2; 0.9 m; 14.1 ± 1.1 ka), T_3 (sample OSL-AR-1; 1.5 m; 37.6 ± 2.1 ka), and one sample from modern channel T_0 sands (sample OSL-AR-3; 0.3 m; 9.1 ± 0.3 ka) were collected (Fig. 6D). Samples belonging to the older age group were collected at depths of > 1 m below the terrace treads of T_1 to T_3 and generally define a younging-trend with increasing height above the modern channel, and T_3 might be a minor fill terrace that is formed by valley aggradation and subsequent channel incision into the alluvium (Fig. 7B). Conversely, the younger age group consists of samples collected at shallow depths (30–90 cm below terrace treads), as well as the T_1 flood plain samples and T_0 samples (Supplement Table S2). In the case of T_1, the shallow and young sample (sample OSL-AR-5; 0.7 m depth; 10.2 ± 0.9 ka) was collected from a sand lens present within a boulder-rich deposit capping the terrace and exhibiting a clear erosional contact with underlying finer-grained and moderately well-sorted sandy pebble conglomerate from which the deeper and older sample (sample OSL-AR-4; 1.7 m depth; 59.2 ± 4.1 ka) was collected (Fig. 7D).

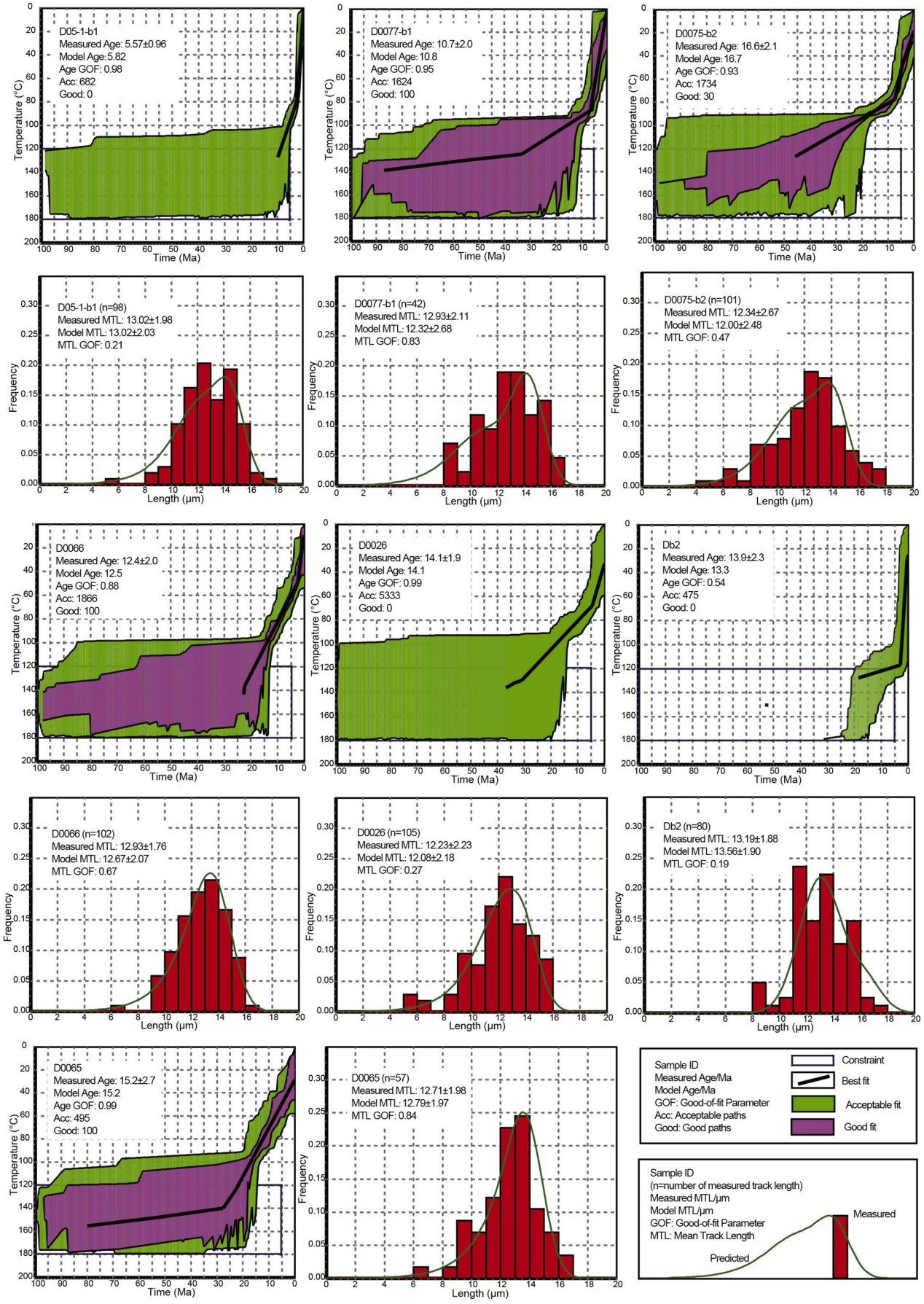

Fig. 10. Apatite fission-track thermal history models and length distributions derived using HeFTy software (Ketcham, 2005).

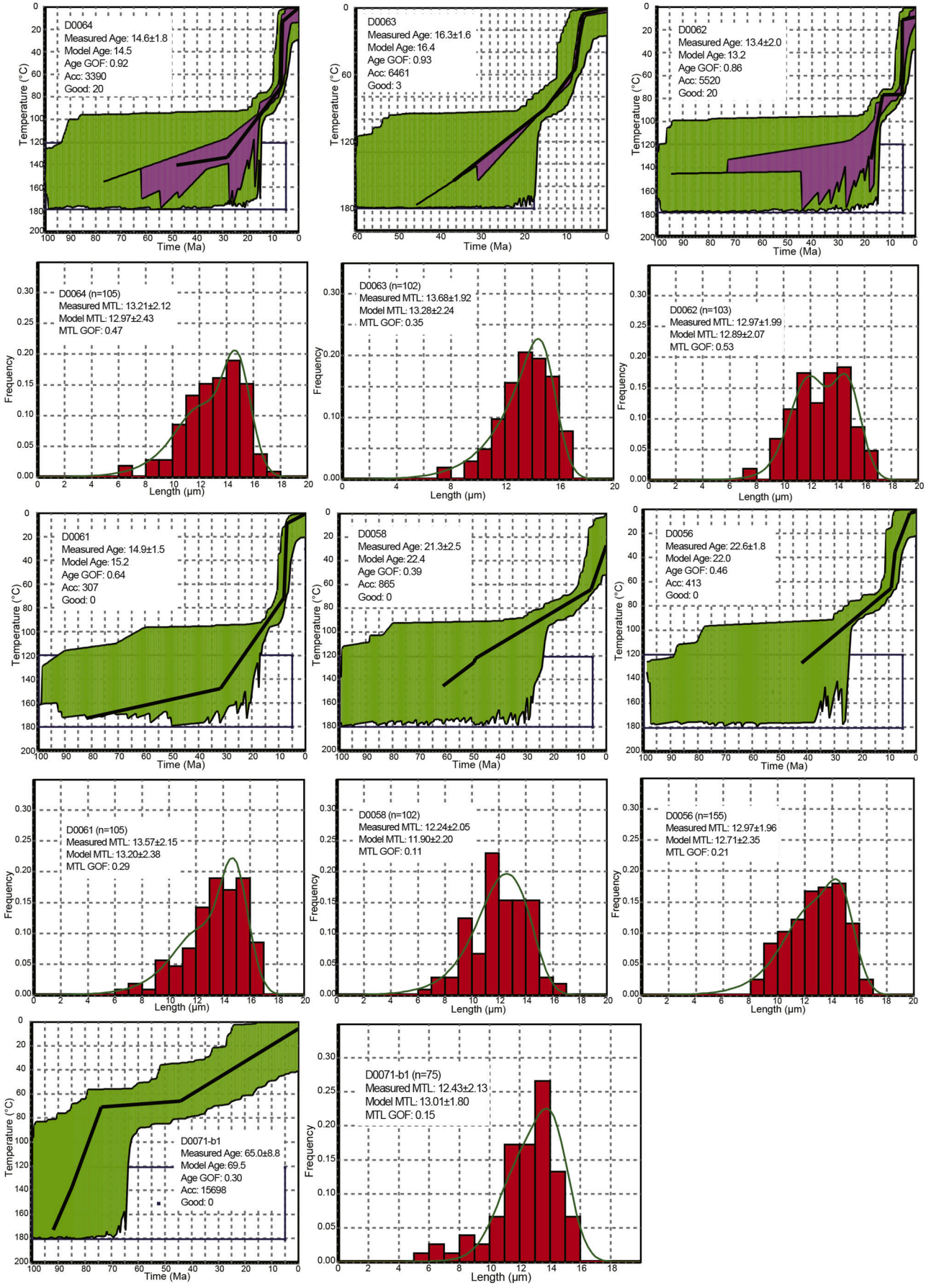

Fig. 10. (*continued*)

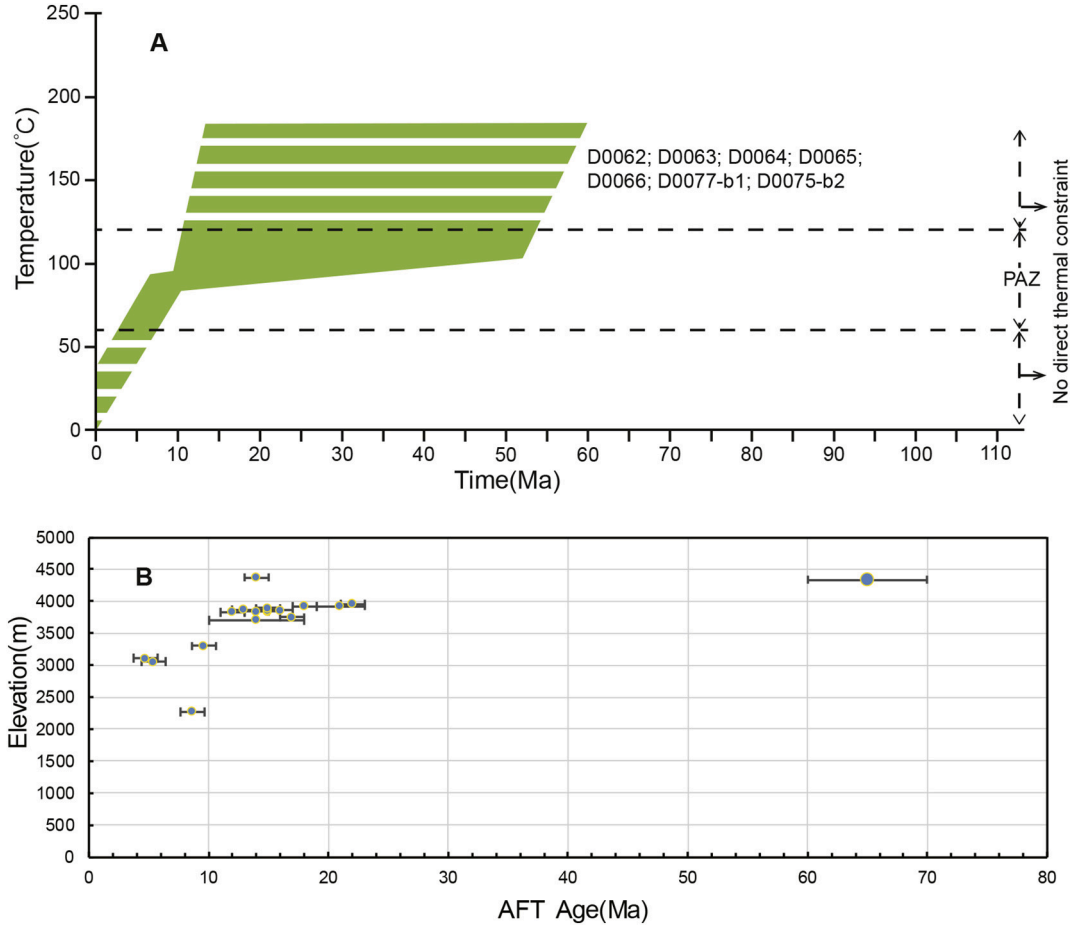

Fig. 11. (A) Summary of thermal history modeling results of samples with good paths in this study and (B) vertical apatite fission-track age-elevation relationship.

8. Discussion

8.1. Cooling history of the western domain of Eastern Kunlun Range

Our new AFT results and thermal history modeling with good paths performed for the samples from the western end of Eastern Kunlun Range suggest two broad cooling events: slow cooling through AFT PAZ since the early Eocene (~55 Ma) and late Miocene rapid cooling (ca. 11–8 Ma) respectively (Fig. 11A). The discrete period of slow cooling since and during the Eocene is consistent with the presence of coarse-grained alluvial conglomerates both in the Fenghuoshan Group of the Hoh Xil Basin and the Lulehe Formation of the Qaidam Basin, which are Paleocene-early Eocene sediments in the Paleo-Qaidam basin (e.g., George et al., 2001; Jolivet et al., 1999, 2001; Liu et al., 2003; Jin et al., 2018; Qinghai BGMR, 1991; Ji et al., 2017). This suggests coupling between the orogenic exhumation and basin infilling, which is contemporaneous with the early stages of the India-Asia collision. Miocene exhumation has been widely reported throughout most of northern Tibet, which is related to rapid surface uplift and exhumation of the Eastern Kunlun Range, the Altyn Tagh Shan, and the Qilian Shan-Nan Shan and activation of strike-slip deformation along the Haiyuan fault (e.g., Duvall et al., 2013; Yuan et al., 2013; Shi et al., 2018; McRivette et al., 2019; L. Wu et al., 2019; Yu et al., 2019a; Wu et al., 2019b; Li et al., 2019, 2020).

Here we consider the timing and magnitude of uplift and exhumation of the Jianxiashan, just south of the Altyn Tagh Shan and the left-slip Altyn Tagh fault. AFT samples were collected along a traverse that paralleled a previously constructed cross-section that shows Cenozoic N-S shortening (Fig. 4B). From this traverse, we constructed an age-elevation profile, which can highlight a preserved AFT PAZ and demonstrate the onset of Miocene rapid cooling (Fig. 11B). AFT ages versus elevation of the Jianxiashan transect show a relatively shallow slope for AFT ages of > 12 Ma, which we interpret to represent a partially preserved AFT PAZ (Fig. 11B). That is, samples collected above 3700 m elevation yield a range of AFT ages from ~12 Ma to ~65 Ma, and thus were at PAZ temperatures for most of the Cenozoic. After ~12 Ma, there is a steep AFT age versus elevation slope, suggesting the initiation of rapid cooling and exhumation (Fig. 11B; Supplement Table S1). These observations suggest that the Jianxiashan mountain range was not significantly deforming or exhuming prior to the middle Miocene.

With this new knowledge of ~12–10 Ma initiation of Jianxiashan thrusting and exhumation, we can present a revised model of Cenozoic shortening. The previous cross-section restoration suggested a minimum of ~24 km Cenozoic shortening (~30% strain) (Fig. 4B) (Wu et al., 2020). Assuming this shortening occurred since ~12–10 Ma yields refined N-S shortening rates of 2.0–2.4 mm/yr and strain rates of 8–9 $\times$ 10^{-16} s^{-1}. These refined rates are not fast enough for Jianxiashan shortening to contribute significantly to left-lateral slip along the Altyn Tagh fault (~10 mm/yr). The derived shortening rates overlap within uncertainties of the Pleistocene-to-present shortening rate of 2.3 $\pm$ 0.9 mm/yr derived by Yakovlev (2015) from Guaizi Liang in the Kumkuli basin (Fig. 1). They are also consistent with other shortening strain rates derived across the Himalayan-Tibetan orogen (e.g., Clark, 2012; Zuza et al., 2018, 2019; Haproff et al., 2019; Wu et al., 2020; Cao et al., 2020).

Other AFT samples not located along the line of cross section exhibit late Miocene (~10 Ma) rapid cooling, as observed by Shi et al. (2018), which may be related to the frontal Qiemo thrusting of the Altyn Tagh Shan. Because left-lateral motion along both the Altyn Tagh fault

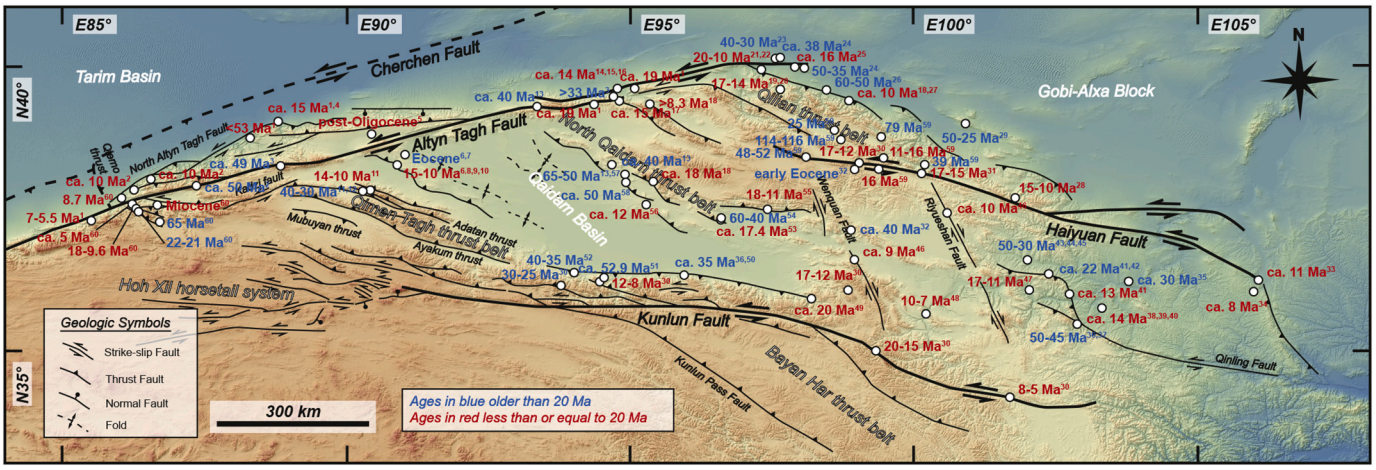

Fig. 12. Topographic map of the northern Tibet with major faults and initial deformation timing, DEM image with 30-m resolution ratio for the base map, initiation ages were derived from: 1-Shi et al. (2018); 2-Jolivet et al. (1999); 3-Yin et al. (2002); 4-Ritts et al. (2008); 5-Yue and Liou (1999); 6- Cheng et al. (2015); 7-Cheng et al. (2016a); 8-Liu et al. (2017a); 9-Chang et al. (2015); 10-Li et al. (2017); 11-Wang et al. (2018); 12-Liu et al. (2017b); 13-Jolivet et al. (2001); 14-Wang et al. (2003); 15-Sun et al. (2005); 16-Lin et al. (2015); 17-Yu et al. (2019a); 18-Zhuang et al. (2018); 19-Yuan et al. (2013); 20-Zheng et al. (2017); 21-Bovet et al. (2009); 22-George et al. (2001); 23-Zhang et al. (2008); 24-An et al. (2020); 25-Wang et al. (2016a); 26-He et al. (2017); 27-Zheng et al. (2010); 28-Li et al. (2019); 29-Zhang et al. (2017); 30-Duvall et al. (2013); 31-Yu et al. (2019b); 32-Qi et al. (2016); 33-Wang et al. (2011); 34-Zheng et al. (2006); 35-Wang et al. (2016b); 36-Clark et al. (2010); 37-Duvall et al. (2011); 38-Fang et al. (2003); 39-Garzione et al. (2005); 40-Hough et al. (2011); 41-Lease et al. (2011); 42-Lease et al. (2012); 43-Dupont-Nivet et al. (2004); 44-Dai et al. (2006); 45-Zhang et al. (2015); 46-Yuan et al. (2011); 47-Yan et al. (2006); 48-Craddock et al. (2011); 49-Yuan et al. (2006); 50-Mock et al. (1999); 51-Chen et al. (2011a); 52-Wang et al. (2017a); 53-Fang et al. (2007); 54-He et al. (2018); 55-Pang et al. (2019); 56-Wang et al. (2017b); 57-Yin et al. (2008a, 2008b); 58-Cheng et al. (2016b); 59- B. Li et al. (2020); 60-This study.

system and the Cherchen fault ceases to the south, all of the lateral motion must be accommodated within the termination of the Qiemo thrust fault. Synchronous deformation and rapid exhumation have been reported along the Qinghai Lake right-slip system, the eastern section of the Kunlun fault, and the Liupan Shan thrust fault (e.g., Zheng et al., 2006; Yuan et al., 2011; Duvall et al., 2013; Shi et al., 2018). However, an average long-term shortening rate of 1.2–0.9 mm/yr since the early Miocene (Wu et al., 2020) in the study area is not enough to contribute to the Altyn Tagh fault displacement, but these thrust faults in the western end of the Eastern Kunlun Range may help distribute shortening from the westernmost Kunlun left-slip fault (Fig. 1).

8.2. Quaternary fluvial terrace development of Aksu drainage and exhumation rate

The OSL dating results from the Aksu drainage may reflect two separate periods of aggradation and incision that occurred during the late Pleistocene and Holocene, respectively. The stratigraphically lowest of the samples, OSL-AR-1 (Fig. 6D), is dated to ~59.2 ka, placing a minimum age constraint on the initiation of alluvial fan construction at Aksu. The youngest ages of this phase are ~37.6 ka from T_3. These ages fall within the range reported for incised valley fill along the Golmud river system (e.g., Wang et al., 2009; Chen et al., 2011b, 2011a; Yu et al., 2020) (Fig. 1) to the east. Wang et al. (2009) and Chen et al. (2011a) present OSL and ^{14}C ages of terrace deposits along the Golmud river system that are as old as ca. 10–13 ka which suggest incision comments prior to this time. Deposits from the inset terrace surfaces at Aksu (T_2 and T_1) has similar OSL ages of ~14.0 ka and 10.2 ka (Supplement Table S2). The youngest material at the Aksu drainage from the T_0 active stream level has a burial age of ~9.1 ka (Supplement Table S2).

The geometry and OSL ages of Quaternary landforms along the Aksu drainage are most consistent with development under the combined effects of climatic variation and tectonic uplift associated with the Cenozoic Indo-Asian collision. If incision and terrace formation are dominantly produced by tectonic uplift, the transition from aggradation to incision must correlate with accelerated uplift. The prolonged river aggradation was succeeded by a phase of fluvial incision that produced the flight of inset terraces observed at the Aksu drainage, a similar two-stage recent history was also proposed for the Golmud river system (Chen et al., 2011b, 2011a). Wang et al. (2009) and Chen et al., 2011b, 2011a suggested that the transition from aggradation to incision correlates with the waning of the last glacial period. Furthermore, Wang et al. (2009) suggested climatic control of discrete terrace formation events and show that incision hiatuses correlate with periods characterized by colder temperatures and/or increased precipitation. Based on the similarities of the observations of those presented herein for the Aksu drainage, the transition to warmer temperatures is interpreted as a primary cause for the termination of regional aggradation. The terraces further developed along the Aksu drainage are interpreted to result from long-term forcing of incision by a constant rate of tectonic uplift modulated by late Quaternary climatic variations (e.g., Wang et al., 2009).

Tectonic uplift is interpreted to drive incision along the northern flank of the Eastern Kunlun Range, and the geometry of geomorphic surfaces produced by incision may be used to calculate a Quaternary (i.e., late Pleistocene-Holocene to present) uplift rate, assuming static base levels. This rate can be driven by either shortening, as shown in the Jianxiashan cross section (Fig. 4B; Wu et al., 2020), proximal uplift adjacent to the left-slip Altyn Tagh fault, or a combination of these processes. At the Aksu drainage, Quaternary uplift rates were estimated from the age of the highest dated surface T_3 surface and the modern stream (T_0) as a reference (Fig. 6D), which yields a rate of 0.9–1.0 mm/yr. We can compare this Quaternary rate to the ~10-Myr uplift rate, by tracking vertical exhumation of the preserved AFT PAZ documented in this study, which occurred at a rate of 0.3–0.5 mm/yr assuming geothermal gradients of 20–30 °C/km. Therefore, the Quaternary exhumation rate (~1 mm/yr) is roughly double the interpreted exhumation rate of the AFT PAZ since ca. 10–12 Ma (0.3–0.5 mm/yr). We interpret that this vertical uplift recorded in the terrace history either reflects a more recent rapid phase of uplift associated with north-south shortening (e.g., Fig. 4B) or vertical uplift driven by the nearby Altyn Tagh fault. We note that Yakovlev (2015) reported vertical Quaternary uplift rates of ~3 mm/yr associated with a fold-thrust system, and so our observed vertical rates may simply reflect a recent phase of fast thrust-related exhumation. However, due to the proximity of the

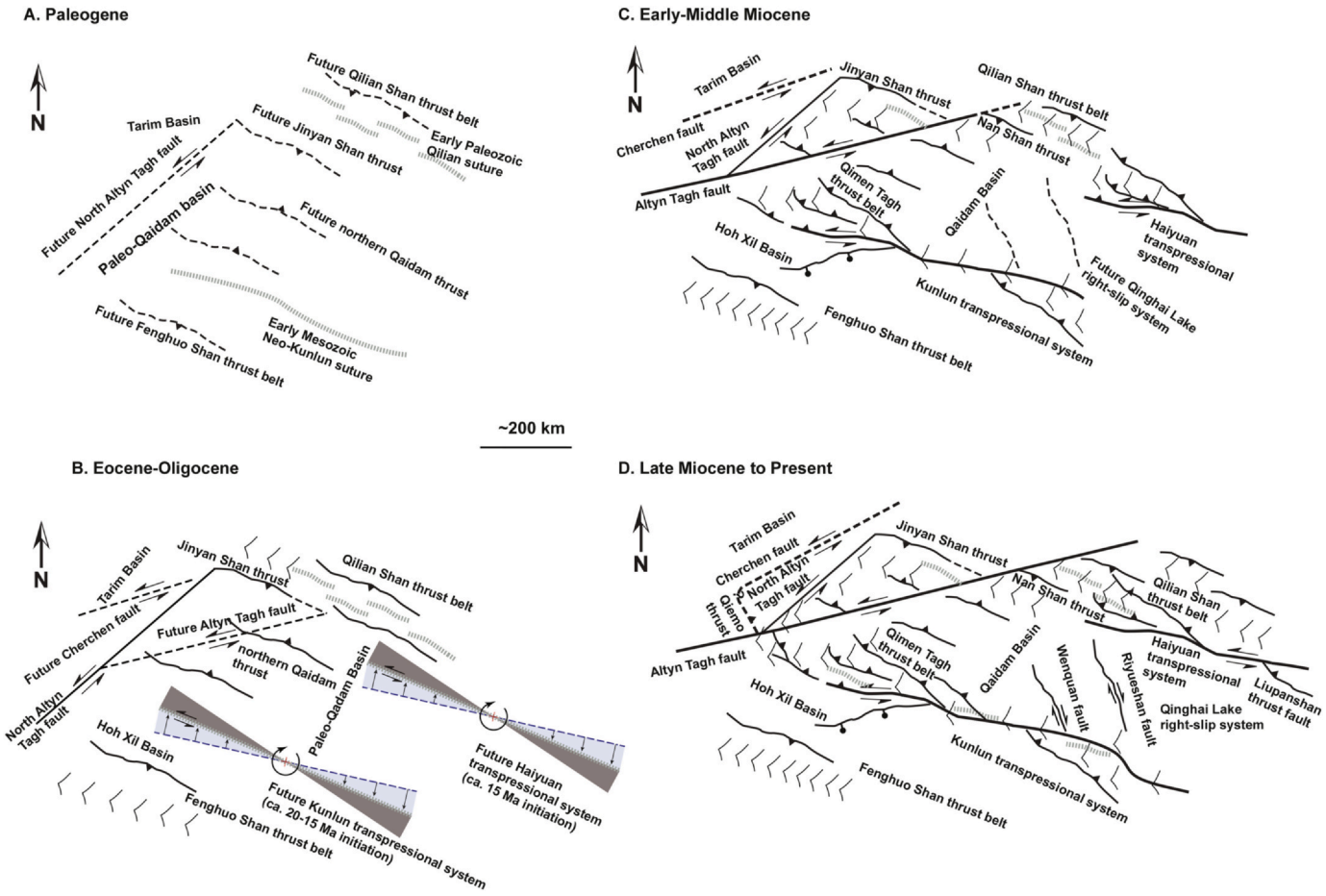

Fig. 13. Proposed tectonic model for the Cenozoic evolution history of the northern Tibet based on this study and published age constraints listed in Fig. 12.

sampling sites to the Altyn Tagh fault, strike-slip related transpressional uplift may be more likely. In either scenario, our data suggests that the rocks around the Aksu river have experienced more rapid exhumation in the Quaternary than over the past ~10 Myr timescales.

8.3. Implications for tectonic evolution of northern Tibet

Together with our new thermochronology data, systematic regional analysis (Fig. 12), and other published datasets, we propose an evolution history and tectonic reconstruction outlined below and shown in Fig. 13. The Paleogene Paleo-Qaidam basin developed in the central-northern Tibet during the Late Mesozoic and Paleogene (e.g., Yin et al., 2008a; McRivette et al., 2019; Wu et al., 2019b; Yu et al., 2020) (Fig. 13A). The North Altyn Tagh fault, Jinyan Shan, and *E*-W-striking thrusts were reactivated by N-S shortening along the pre-existing crustal weaknesses formed originally in the early Paleozoic and/or late Mesozoic (e.g., Sobel and Arnaud, 1999; Chen et al., 2003; Cowgill et al., 2000, 2003; Zhang et al., 2017b, 2017a; L. Wu et al., 2019). Uplift and deformation of the late Mesozoic strata in the Paleo-Qaidam basin was associated with the initiation of thrusting within the Fenghuo Shan thrust belt in the south and the Qilian Shan thrust belt in the north, which occurred no later than the early Eocene (e.g., Leeder et al., 1988; Jolivet et al., 1999, 2001; Horton et al., 2004; Spurlin et al., 2005; Yin et al., 2008a; Wu et al., 2011; Zhuang et al., 2011, 2018; Yuan et al., 2013; Li et al., 2020) (Figs. 12 and 13B). Deformation along the northern plateau margin clearly started early after initial India-Asia collision, before exhumation observed in the western Eastern Kunlun Range (Shi et al., 2018; this study). These observations support out-of-sequence models for Tibetan Plateau growth (e.g., Jolivet et al., 2001; Li et al., 2020; Bian et al., 2020), instead of northward propagating deformation models (e.g., Tapponnier et al., 2001).

Thermochronology data and sediment provenance analysis indicates a northward propagation of the Early Miocene Altyn Tagh fault, and the subsequent rapid exhumation may have been related to the initial uplift of the Nanshan region (e.g., Cowgill et al., 2000, 2003; Shi et al., 2018; L. Wu et al., 2019; Yu et al., 2019a) (Figs. 12 and 13C). Slip along both the left-slip Altyn Tagh fault and Cherchen fault control the uplift and southward growth of the Altyn Tagh Shan.

Reactivation of a preexisting plane of weakness (i.e., early Mesozoic Neo-Kunlun suture, e.g., Wu et al., 2016) with a northeast-southwest maximum horizontal compressive stress direction is expected to induce left-lateral shearing, consistent with the kinematics of the Cenozoic Kunlun transpressional system during the Miocene, which resulted in the onset of Cenozoic uplift of the Eastern Kunlun Range (e.g., Yin et al., 2008a; Zuza and Yin, 2016; Zuza et al., 2017; Wu et al., 2019a, 2019b) (Fig. 13C). In addition, the Haiyuan fault, which initiated at ~15 Ma as constrained along the western and central segments (e.g., Yu et al., 2019b; Li et al., 2019, 2020), shows a similar transpressional structure linked with Qilian Shan-Nan Shan thrusts (Fig. 13C). Rapid exhumation of the southwest Altyn Tagh Shan occurred at ~10 Ma (Jolivet et al., 1999), in addition to rapid exhumation of the study area initiating in the Late Miocene (Shi et al., 2018; this study). We suggest a possibility for the Qiemo thrust linked with the Cherchen fault and the Altyn Tagh fault as the frontal thrust of the uplifting and southward growing Altyn Tagh Shan (Fig. 13D). Thermochronology age constraints for the initiation of deformation within the Kunlun fault system indicate that all components of the system has been contemporaneously active since at least the late Miocene, including the Qinghai Lake right-slip fault system that is bounded by the Kunlun and Haiyuan left-slip faults, i.e., the Wenquan and Riyueshan right-slip faults (Wu et al., 2019a; Figs. 12

and 13D).

Geometric and kinematic considerations demonstrate that this contractional deformation within the western end of Eastern Kunlun Range did not significantly contribute to left-slip offset on the Altyn Tagh fault (Cowgill, 2007; Wu et al., 2020; Fig. 13D). The range-bounding SSW-directed thrust faults in the central Qilian Shan merge to the southeast with the Haiyuan fault (Zuza et al., 2018; Li et al., 2020; Fig. 13D). The western end of the Eastern Kunlun Range may similarly diffuse strike-slip displacement on the Kunlun fault. Therefore thrusts within the Eastern Kunlun Range do not contribute to the left-slip Altyn Tagh fault (Wu et al., 2020; this study), but may accommodate kinematically linked left-slip motion along the Kunlun fault, similar to the Haiyuan fault (Fig. 13D). The deformation pattern in northern Tibet results from clockwise rotation of left-slip fault-reactivated preexisting weaknesses (i.e., the suture zones) and broad transpressional systems between the Kunlun and Haiyuan faults. In this framework, the Qinghai Lake right-slip faults are rotation/bookshelf structures within this broader rotating system (Fig. 13C and D).

9. Conclusions

In this study, we present new field observations, AFT data, and OSL ages from the relatively understudied junction of the Eastern Kunlun Range and Altyn Tagh Shan in northern Tibet. Apatite fission-track ages can be divided into three domains with different mean ages: Paleocene (~65 Ma), Miocene (ca. 22–8.7 Ma), and early Pliocene (ca. 5.4–4.7 Ma). These cooling ages and thermal history modeling results suggest that the study area experienced two broad cooling events: slow cooling through AFT PAZ from the early Eocene (~55 Ma) and late Miocene rapid cooling (ca. 11–8 Ma). AFT samples from the Jianxiashan thrust system display a paleo-PAZ that was exhumated via thrusting starting at ca. 10–12 Ma. This timing constraint allows refinement of previously published north-south late Miocene shortening rates on this thrust system to ~2 mm/yr, which we argue does not significantly contribute to left-slip faulting on the Altyn Tagh fault.

Our OSL dating results from the Aksu drainage reflect two separate periods of aggradation and incision that occurred during the late Pleistocene and Holocene, respectively. The terraces along the Aksu drainage are interpreted to result from long-term forcing of incision during a constant rate of tectonic uplift modulated by late Quaternary climatic variations. We interpret that this incision occurred at a rate of ~1 mm/yr, which is faster than exhumation rates inferred from the AFT data (0.3–0.5 mm/yr). These fast Quaternary exhumation rates may reflect recent exhumation or uplift associated transpression along the proximal Altyn Tagh fault.

In accordance with previous studies, we present a refined Cenozoic tectonic model for the evolution history of the northern Tibet. Although deformation started early in the Eocene along the northern plateau margin in the Qilian Shan, deformation and exhumation in the study area did not initiate until the Miocene. These observations support out-of-sequence development of the northern Tibetan Plateau. Miocene exhumation and deformation in the western Eastern Kunlun Range resulted from activation of a major preexisting weakness (i.e., suture zone) during regional clockwise rotation, which established the present-day deformation pattern in northern Tibet, consisting of the broad transpressional left-slip fault systems along the Kunlun and Haiyuan faults.

Declaration of Competing Interest

The authors declare that they have no known competing financial interests or personal relationships that could have appeared to influence the work reported in this paper.

Acknowledgements

This research was supported by grants from the Second Tibetan Plateau Scientific Expedition and Research Program (Grant No. 2019QZKK0708), the Basic Science Center for Tibetan Plateau Earth System (CTPES, Grant 41988101-01), National Natural Science Foundation of China (Grants Nos. 41702232, 41941016, 41661134049), the National Key Research and Development Project of China (Grant No. 2016YFC0600303), the Chinese Academy of Sciences, Strategic Priority Research Program (Grant No. XDA20070301), the China Geological Survey (DD20160083) and the NSF Tectonics program of the National Science Foundation (EAR 1914501) (A. Zuza). We appreciate the Editor, Dr. Feng Cheng, Dr. Peter Haproff, and five anonymous reviewers for their critical, careful, and very constructive reviews that helped to improve the clarity and interpretations of the original draft.

Appendix A. Supplementary data

Supplementary data to this article can be found online at https://doi.org/10.1016/j.palaeo.2020.109971.

References

An, K., Lin, X., Wu, L., Yang, R., Chen, H., Cheng, X., Xia, Q., Zheng, F., Ding, W., Gao, S., Li, C., Zhang, Y., 2020. An immediate response to the Indian-Eurasian collision along the northeastern Tibetan Plateau: evidence from apatite fission track analysis in the Kuantan Shan-Hei Shan. Tectonophysics 774, 228–278. https://doi.org/10.1016/j.tecto.2019.228278.

Bian, S., Gong, J., Chen, L., Zuza, A.V., Chen, H., Lin, X., Cheng, X.G., Yang, R., 2020. Diachronous uplift in intra-continental orogeny: 2D thermo-mechanical modeling of the India-Asia collision. Tectonophysics 775, 228310. https://doi.org/10.1016/j.tecto.2019.228310. (in press).

Bilham, R., Gaur, V.K., Molnar, P., 2001. Himalayan seismic hazard. Science 293 (5534), 1442–1444.

Bovet, P.M., Ritts, B.D., Gehrels, G., Abbink, A.O., Darby, B., Hourigan, J., 2009. Evidence of Miocene crustal shortening in the north Qilian Shan from Cenozoic stratigraphy of the western Hexi Corridor, Gansu Province, China. Am. J. Sci. 309 (4), 290–329. https://doi.org/10.2475/00.4009.02.

Brooks, Benjamin A., Bevis, Michael, Kelin, Whipple, Ramon Arrowsmith, J., Foster, James, Zapata, Tomas, Kendrick, Eric, et al., 2011. Orogenic-wedge deformation and potential for great earthquakes in the central Andean backarc. Nat. Geosci. 4 (6), 380–383.

Burchfiel, B.C., Deng, Q.D., Molnar, P., Royden, L., Wang, Y.P., Zheng, P.Z., Zhang, W.Q., 1989. Intracrustal detachment within zones of continental deformation. Geology 17, 748–752. https://doi.org/10.1130/0091-7613(1989)017<0448:IDWZOC>2.3.CO;2.

Cao, W., Yang, J., Zuza, A.V., Ji, W.Q., Ma, X.X., Chu, X., Burgess, Q.P., 2020. Crustal tilting and differential exhumation of Gangdese Batholith in southern Tibet revealed by bedrock pressures. Earth Planet. Sci. Lett. 543, 116347.

Chang, H., Li, L., Qiang, X., Garzione, C.N., Pullen, A., An, Z., 2015. Magnetostratigraphy of Cenozoic deposits in the western Qaidam Basin and its implication for the surface uplift of the northeastern margin of the Tibetan Plateau. Earth Planet. Sci. Lett. 430, 271–283. https://doi.org/10.1016/j.epsl.2015.08.029.

Che, Z., Liu, L., Luo, J.H., 1995. The discovery and occurrence of high-pressure metamorphic rocks from Altyn Mountain area, Xinjiang Autonomous Region. Chin. Sci. Bull. 40, 1298–1300 (in Chinese).

Chen, W.P., Chen, C.Y., Nabelek, J.L., 1999. Present-day deformation of the Qaidam Basin with implications for intra-continental tectonics. Tectonophysics 305, 165–181. https://doi.org/10.1016/S0040-1951(99)00006-2.

Chen, X.H., Yin, A., Gehrels, G.E., Cowgill, E.S., Grove, M., Harrison, T.M., Wang, X.F., 2003. Two phases of Mesozoic north-south extension in the eastern Altyn Tagh range, northern Tibetan Plateau. Tectonics 22 (5), 1–22. https://doi.org/10.1029/2001TC001336.

Chen, X.H., Dang, Y.Q., Yin, A., Wang, L.Q., Jiang, W.M., Li, L., 2010. Basin Mountain Coupling and Tectonic Evolution of Qaidam Basin and its Adjacent Orogenic Belts. Geological Publishing House, Beijing, pp. 1–365 (in Chinese).

Chen, X.H., McRivette, M.W., Li, L., Yin, A., Jiang, R.B., Wan, J.L., Li, H.J., 2011b. Thermochronological evidence for multi-phase uplifting of the east Kunlun Mountains, northern Tibetan Plateau. Geol. Bull. China 30, 1647–1660 (in Chinese with English abstract).

Chen, Y., Li, Y., Zhang, Y., Zhang, M., Zhang, J., Yi, C., Liu, G., 2011a. Late Quaternary deposition and incision sequences of the Golmud River and their environmental implications. Quat. Int. 236 (1–2), 48–56. https://doi.org/10.1016/j.quaint.2010.05.028.

Cheng, F., Guo, Z., Jenkins, H.S., Fu, S., Cheng, X., 2015. Initial rupture and displacement on the Altyn Tagh fault, northern Tibetan Plateau: constraints based on residual Mesozoic to Cenozoic strata in the western Qaidam Basin. Geosphere 11 (3),

921–942. https://doi.org/10.1130/GES01070.1.
Cheng, F., Jolivet, M., Fu, S., Zhang, C., Zhang, Q., Guo, Z., 2016a. Large-scale displacement along the Altyn Tagh Fault (North Tibet) since its Eocene initiation: insight from detrital zircon U-Pb geochronology and subsurface data. Tectonophysics 677–678, 261–279. https://doi.org/10.1016/j.tecto.2016.04.023.
Cheng, X.G., Lin, X.B., Wu, L., Chen, H.L., Xiao, A.C., Gong, J.F., Zhang, F.Q., Yang, S.F., 2016b. The exhumation history of North Qaidam Thrust Belt constrained by apatite fission track thermochronology: implication for the evolution of the Tibetan Plateau. Acta Geol. Sin. 90 (3), 870–883. https://doi.org/10.1111/1755-6724.12730. English Edition.
Clark, M.K., 2012. Continental collision slowing due to viscous mantle lithosphere rather than topography. Nature 483, 74–77. https://doi.org/10.1038/nature10848.
Clark, M.K., Farley, K.A., Zheng, D., Wang, Z., Duvall, A.R., 2010. Early Cenozoic faulting of the northern Tibetan Plateau margin from apatite (U-Th)/He ages. Earth Planet. Sci. Lett. 296 (1–2), 78–88. https://doi.org/10.1016/j.epsl.2010.04.051.
Cowgill, E., 2007. Impact of riser reconstructions on estimation of secular variation in rates of strike-slip faulting: revisiting the Cherchen River site along the Altyn Tagh fault, NW China. Earth Planet. Sci. Lett. 254 (3–4), 239–255. https://doi.org/10.1016/j.epsl.2006.09.015.
Cowgill, E., Yin, A., Wang, X.F., Zhang, Q., 2000. Is the North Altyn fault part of a strike-slip duplex along the Altyn Tagh fault system? Geology 28, 255–258. https://doi.org/10.1130/0091-7613(2000)28<255:ITNAFP>2.0.CO;2.
Cowgill, E., Yin, A., Harrison, T.M., Wang, X.F., 2003. Reconstruction of the Altyn Tagh fault based on U-Pb geochronology: role of back thrusts, mantle sutures, and heterogeneous crustal strength in forming the Tibetan Plateau. J. Geophys. Res. 108, 2346. https://doi.org/10.1029/2002JB002080.
Cowgill, E., Gold, R.D., Xuanhua, C., Xiao-Feng, W., Arrow-smith, J.R., Southon, J., 2009. Low Quaternary slip rate reconciles geodetic and geologic rates along the Altyn Tagh fault, northwestern Tibet. Geology 37 (7), 647–650. https://doi.org/10.1130/G25623A.1.
Craddock, W., Kirby, E., Zhang, H., 2011. Late Miocene-Pliocene range growth in the interior of the northeastern Tibetan Plateau. Lithosphere 3 (6), 420–438. https://doi.org/10.1130/L159.1.
Dai, S., Fang, X., Dupont-Nivet, G., Song, C., Gao, J., Krijgsman, W., et al., 2006. Magnetostratigraphy of Cenozoic sediments from the Xining Basin: tectonic implications for the northeastern Tibetan Plateau. J. Geophys. Res. 111 (B11102). https://doi.org/10.1029/2005JB004187.
Donelick, R.A., Miller, D.S., 1991. Enhanced TINT fission track density apatites using ^{252}Cf-derived fission fragment tracks: a model and experimental observations. Nucl. Tracks Radiat. Meas. 18, 301–307. https://doi.org/10.1016/1359-0189(91)90022-A.
Dupont-Nivet, G., Horton, B.K., Butler, R.F., Wang, J., Zhou, J., Waanders, G.L., 2004. Paleogene clockwise tectonic rotation of the Xining-Lanzhou region, northeastern Tibetan Plateau. J. Geophys. Res. 109 (B04401). https://doi.org/10.1029/2003JB002620.
Duvall, A.R., Clark, M.K., van der Pluijm, B.A., Li, C., 2011. Direct dating of Eocene reverse faulting in north-eastern Tibet using Ar-dating of fault clays and low-temperature thermochronometry. Earth Planet. Sci. Lett. 304 (3–4), 520–526. https://doi.org/10.1016/j.epsl.2011.02.028.
Duvall, A.R., Clark, M.K., Kirby, E., Farley, K.A., Craddock, W.H., Li, C., Yuan, D.Y., 2013. Low-temperature thermochronometry along the Kunlun and Haiyuan Faults, NE Tibetan Plateau: evidence for kinematic change during late-stage orogenesis. Tectonics 32 (5), 1190–1211. https://doi.org/10.1002/tect.20072.
Fang, X., Garzione, C., Van der Voo, R., Li, J., Fan, M., 2003. Flexural subsidence by 29 Ma on the NE edge of Tibet from the magnetostratigraphy of Linxia Basin, China. Earth Planet. Sci. Lett. 210 (3–4), 545–560. https://doi.org/10.1016/S0012-821X(03)00142-0.
Fang, X., Zhang, W., Meng, Q., Gao, J., Wang, X., King, J., et al., 2007. High-resolution magnetostratigraphy of the Neogene Huaitoutala section in the eastern Qaidam Basin on the NE Tibetan Plateau, Qinghai Province, China and its implication on tectonic uplift of the NE Tibetan Plateau. Earth Planet. Sci. Lett. 258 (1–2), 293–306. https://doi.org/10.1016/j.epsl.2007.03.042.
Galbraith, R.F., 1990. The radial plot: graphical assessment of spread in ages. Int. J. Radiat. Appl. Instrum. D 17, 207–214. https://doi.org/10.1016/1359-0189(90)90036-W.
Garzione, C.N., Ikari, M.J., Basu, A.R., 2005. Source of Oligocene to Pliocene sedimentary rocks in the Linxia basin in northeastern Tibet from Nd isotopes: implications for tectonic forcing of climate. Geol. Soc. Am. Bull. 117 (9), 1156–1166. https://doi.org/10.1130/B25743.1.
Garzione, C.N., Mcquarrie, N., Perez, N.D., Ehlers, T.A., Beck, S.L., Kar, N., et al., 2017. Tectonic evolution of the central andean plateau and implications for the growth of plateaus. Annu. Rev. Earth Planet. Sci. 45 (1) annurev-earth-063016-020612.
George, A.D., Marshallsea, S.J., Wyrwoll, K.H., Chen, J., Lu, Y., 2001. Miocene cooling in the northern Qilian Shan, northeastern margin of the Tibetan Plateau, revealed by apatite fission-track and vitrinite-reflectance analysis. Geology 29 (10), 939–942. https://doi.org/10.1130/0091-7613(2001)029<0939:MCITNQ>2.0.CO.
Gleadow, A.J., Kohn, B.P., Brown, R.W., O'Sullivan, P.B., Raza, A., 2002. Fission track thermotectonic imaging of the Australian continent. Tectonophysics 349 (1–4), 5–21. https://doi.org/10.1016/S0040-1951(02)00043-4.
Gleadow, A.J.W., 1981. Fission-track dating methods: what are the real alternatives? Nucl. Tracks 5, 3–14. https://doi.org/10.1016/0191-278X(81)90021-4.
Gleadow, A.J.W., Duddy, I.R., Green, P.F., Lovering, J.F., 1986. Confined fission track lengths in apatite: a diagnostic tool for thermal history analysis. Contrib. Mineral. Petrol. 94, 405–415. https://doi.org/10.1007/BF00376334.
Green, P.F., Duddy, I.R., Gleadow, A.J.W., Laslett, G.M., Tingate, P.R., 1986. Thermal annealing of fission track in apatite 1: a qualitative description. Chem. Geol. 59, 237–253. https://doi.org/10.1016/0168-9622(86)90074-6.
Haproff, P.J., Zuza, A.V., Yin, A., Harrison, T.M., Manning, C.E., Dubey, C.S., Ding, L., Wu, C., Chen, J., 2019. Geologic framework of the northern Indo-Burma Ranges and lateral correlation of Himalayan-Tibetan lithologic units across the eastern Himalayan syntaxis. Geosphere 15 (3), 856–881. https://doi.org/10.1130/GES02054.1.
He, P., Wang, X., Song, C., Wang, Q., Deng, L., Zhong, S., 2017. Cenozoic evolution of the Western Qinling Mt. Range based on thermochronologic and sedimentary records from the Wudu Basin, NE Tibetan Plateau. J. Asian Earth Sci. 138, 484–494. https://doi.org/10.1016/j.jseaes.2017.02.033.
He, P., Song, C., Wang, Y., Meng, Q., Chen, L., Yao, L., et al., 2018. Cenozoic deformation history of the Qilian Shan (northeastern Tibetan Plateau) constrained by detrital apatite fission-track thermochronology in the northeastern Qaidam Basin. Tectonophysics 749, 1–11. https://doi.org/10.1016/j.tecto.2018.10.017.
Horton, B.K., Dupont-Nivet, G., Zhou, J., Waanders, G.L., Butler, R.F., Wang, J., 2004. Mesozoic-Cenozoic evolution of the Xining-Minhe and Dangchang basins, northeastern Tibetan Plateau: magnetostratigraphic and biostratigraphic results. J. Geophys. Res. 109 (B04402). https://doi.org/10.1029/2003JB002913.
Hough, B.G., Garzione, C.N., Wang, Z., Lease, R.O., Burbank, D.W., Yuan, D., 2011. Stable isotope evidence for topographic growth and basin segmentation: implications for the evolution of the NE Tibetan Plateau. Geol. Soc. Am. Bull. 123 (1–2), 168–185. https://doi.org/10.1130/B30090.1.
Hurford, A.J., 1990. Standardization of fission track dating calibration: recommendation by the Fission Track Working Group of the IUGS Subcommission on Geochronology. Chem. Geol. Isot. Geosci. 80, 171–178. https://doi.org/10.1016/0168-9622(90)90025-8.
Hurford, A.J., Green, P.F., 1983. The zeta age calibration of fission-track dating. Chem. Geol. 41, 285–317. https://doi.org/10.1016/S0009-2541(83)80026-6.
Ji, J., Zhang, K., Clift, P.D., Zhuang, G., Song, B., Ke, X., 2017. High-resolution magnetostratigraphic study of the Paleogene-Neogene strata in the northern Qaidam basin: implications for the growth of the northeastern Tibetan plateau. Gondwana Res. 46, 141–155. https://doi.org/10.1016/j.gr.2017.02.015.
Jiao, D.Y., Liu, C.F., Liu, W.C., Su, H., He, J.L., Zhao, Z.X., Ye, B.Y., Xu, X., 2020. Petrogenesis and tectonic significance of the late Devonian-early Carboniferous Jianxiashan pluton in the western domain of the eastern Kunlun Orogen, northern Tibetan Plateau. Geol. J. https://doi.org/10.1002/gj.3804. (in press).
Jin, C., Liu, Q., Liang, W., Roberts, A.P., Sun, J., Hu, P., Duan, Z., 2018. Magnetostratigraphy of the Fenghuoshan Group in the Hoh Xil Basin and its tectonic implications for India-Eurasia collision and Tibetan Plateau deformation. Earth Planet. Sci. Lett. 486, 41–53. https://doi.org/10.1016/j.epsl.2018.01.010.
Jolivet, M., Brunel, M., Seward, D., Xu, Z., Yang, J., Roger, F., Wu, C., 2001. Mesozoic and Cenozoic tectonics of the northern edge of the Tibetan Plateau: fission-track constraints. Tectonophysics 343 (1–2), 111–134. https://doi.org/10.1016/S0040-1951(01)00196-2.
Jolivet, M., Brunel, M., Roger, F., Tapponnier, P., Arnaud, N., Seward, D., 1999. Exhumation history of the Altun Shan with evidence for the timing of the subduction of the Tarim block beneath the Altyn Tagh system, North Tibet. Earth Planet. Sci. 329 (10), 749–755.
Jolivet, M., Brunel, M., Seward, D., Xu, Z., Yang, J., Malavieille, J., et al., 2003. Neogene extension and volcanism in the kunlun fault zone, northern tibet: new constraints on the age of the kunlun fult. Tectonics 22 (5).
Kang, L., Xiao, P.X., Gao, X.F., Xi, R.G., Yang, Z.C., 2016. Early Paleozoic magmatism and collision orogenic process of the South Altyn. Acta Geol. Sin. 90, 2527–2550 (in Chinese with English abstract).
Kapp, P., Pelletier, J.D., Rohrmann, A., Heermance, R., Russell, J., Ding, L., 2011. Wind erosion in the Qaidam basin, central Asia: implications for tectonics, paleoclimate, and the source of the Loess Plateau. GSA Today 21 (4–5), 4–10. https://doi.org/10.1130/gsatg99a.1.
Ketcham, R.A., 2005. Forward and inverse modeling of low-temperature thermochronometry data. Rev. Mineral. Geochem. 58, 275–314. https://doi.org/10.2138/rmg.2005.58.11.
Ketcham, R.A., Carter, A., Donelick, R.A., Barbarand, J., Hurford, A.J., 2007. Improved modeling of fission-track annealing in apatite. Am. Mineral. 92 (5–6), 799–810. https://doi.org/10.2138/am.2007.2281.
Kirby, E., Whipple, K.X., 2001. Quantifying differential rock-uplift rates via stream profile analysis. Geology 29, 415–418. https://doi.org/10.1130/0091-7613(2001)029<0415:QDRURV>2.0.CO;2.
Laslett, G.M., Green, P.F., Duddy, I.R., Gleadow, A.J.W., 1987. Thermal annealing of fission tracks in apatite 2: a quantitative analysis. Chem. Geol. Isot. Geosci. 65, 1–13. https://doi.org/10.1016/0168-9622(87)90057-1.
Lease, R.O., Burbank, D.W., Clark, M.K., Farley, K.A., Zheng, D., Zhang, H., 2011. Middle Miocene reorganization of deformation along the northeastern Tibetan Plateau. Geology 39 (4), 359–362. https://doi.org/10.1130/G31356.1.
Lease, R.O., Burbank, D.W., Hough, B., Wang, Z., Yuan, D., 2012. Pulsed Miocene range growth in northeastern Tibet: insights from Xunhua Basin magnetostratigraphy and provenance. Geol. Soc. Am. Bull. 124 (5–6), 657–677. https://doi.org/10.1130/B30524.1.
Leeder, M.R., Smith, A.B., Yin, J., 1988. Sedimentology, palaeoecology and palaeoenvironmental evolution of the 1985 Lhasa to Golmud Geotraverse. Philosophical Transactions of the Royal Society of London. Series A. Math. Phys. Sci. 327, 107–143. https://doi.org/10.1098/rsta.1988.0123.
Li, B., Yan, M., Zhang, W., Fang, X., Meng, Q., Zan, J., et al., 2017. New paleomagnetic constraints on middle Miocene strike-slip faulting along the middle Altyn Tagh Fault. J. Geophys. Res. Solid Earth 122, 4106–4122. https://doi.org/10.1002/2017JB014058.
Li, B., Chen, X., Zuza, A.V., Hu, D., Ding, W., Huang, P., Xu, S., 2019. Cenozoic cooling history of the North Qilian Shan, northern Tibetan Plateau, and the initiation of the

Haiyuan fault: constraints from apatite-and zircon-fission track thermochronology. Tectonophysics 751, 109–124. https://doi.org/10.1016/j.tecto.2018.12.005.
Li, B., Zuza, A.V., Chen, X., Hu, D., Shao, Z., Qi, B., Wang, Z., Levy, D.A., Xiong, X., 2020. Cenozoic multi-phase deformation in the Qilian Shan and out-of-sequence development of the northern Tibetan Plateau. Tectonophysics 782–783, 228423. (in press). https://doi.org/10.1016/j.tecto.2020.228423.
Lin, X., Zheng, D., Sun, J., Windley, B.F., Tian, Z., Gong, Z., Jia, Y., 2015. Detrital apatite fission track evidence for provenance change in the Subei Basin and implications for the tectonic uplift of the Danghenan Shan (NW China) since the mid-Miocene. J. Asian Earth Sci. 111, 302–311. https://doi.org/10.1016/j.jseaes.2015.07.007.
Liu, D., Li, H., Sun, Z., Pan, J., Wang, M., Wang, H., 2017b. AFT dating constrains the Cenozoic uplift of the Qimen Tagh Mountains, Northeast Tibetan Plateau, comparison with LA-ICPMS Zircon U-Pb ages. Gondwana Res. 41, 438–450. https://doi.org/10.1016/j.gr.2015.10.008.
Liu, L., Kang, L., Cao, Y., Yang, W., 2015. Early Paleozoic granitic magmatism related to the processes from subduction to collision in South Altyn, NW China. Sci. China Earth Sci. 58 (9), 1513–1522. https://doi.org/10.1007/s11430-015-5151-1.
Liu, R., Allen, M.B., Zhang, Q., Du, W., Cheng, X., Holdsworth, R.E., Guo, Z., 2017a. Basement controls on deformation during oblique convergence: transpressive structures in the western Qaidam Basin, northern Tibetan Plateau. Lithosphere 9 (4), 583–594. https://doi.org/10.1130/L634.1.
Liu-Zeng, J., Tapponnier, P., Gaudemer, Y., Ding, L., 2008. Quantifying landscape differences across the tibetan plateau: implications for topographic relief evolution. J. Geophys. Res. 113 (F4), F04018.
Liu, Z.F., Zhao, X., Wang, C.S., Liu, S., Yi, H., 2003. Magnetostratigraphy of Tertiary sediments from the Hoh Xil basin: implications for the Cenozoic tectonic history of the Tibetan plateau. Geophys. J. Int. 154, 233–252. https://doi.org/10.1046/j.1365-246X.2003.01986.x.
McRivette, M.W., Yin, A., Chen, X., Gehrels, G.E., 2019. Cenozoic basin evolution of the central Tibetan plateau as constrained by U-Pb detrital zircon geochronology, sandstone petrology, and fission-track thermochronology. Tectonophysics 751, 150–179. https://doi.org/10.1016/j.tecto.2018.12.015.
Meyer, B., Tapponnier, P., Bourjot, L., Metivier, F., Gaudemer, Y., Peltzer, G., Shunmin, G., Zhitai, C., 1998. Crustal thickening in Gansu-Qinghai, lithospheric mantle subduction, and oblique, strike-slip controlled growth of the Tibet plateau. Geophys. J. Int. 135 (1), 1–47. https://doi.org/10.1046/j.1365-246X.1998.00567.x.
Mock, C., Arnaud, N.O., Cantagrel, J.M., 1999. An early unroofing in northeastern Tibet? Constraints from $^{40}Ar/^{39}Ar$ thermochronology on granitoids from the Eastern Kunlun Range (Qianghai, NW China). Earth Planet. Sci. Lett. 171, 107–122. https://doi.org/10.1016/S0012-821X(99)00133-8.
Molnar, P., 1988. Continental tectonics in the aftermath of plate tectonics. Nature 335, 131–137. https://doi.org/10.1038/335131a0.
Molnar, P., Stock, J.M., 2009. Slowing of India's convergence with Eurasia since 20 Ma and its implications for Tibetan mantle dynamics. Tectonics 28, TC3001. https://doi.org/10.1029/2008TC002271.
Molnar, P., Boos, W.R., Battisti, D.S., 2010. Orographic controls on climate and paleoclimate of Asia: thermal and mechanical roles for the Tibetan Plateau. Ann. Rev. Earth Planet. Sci. 38 (1), 77–102. https://doi.org/10.1146/annurev-earth-040809-152456.
Owen, L.A., Finkel, R.C., Haizhou, M., Barnard, P.L., 2006. Late Quaternary landscape evolution in the Kunlun Mountains and Qaidam Basin, Northern Tibet: a framework for examining the links between glaciation, lake level changes and alluvial fan formation. Quat. Int. 154–155, 73–86. https://doi.org/10.1016/j.quaint.2006.02.008.
Pan, G.T., Ding, J., Yao, D., Wang, L., 2004. Geological Map of Qinghai-Xiang (Tibet) Plateau and Adjacent Areas: Chengdu Institute of Geology and Mineral Resources: China Geological Survey, Chengdu, Chengdu Cartographic Publishing House, Scale 1:1,500,000.
Pang, J., Yu, J., Zheng, D., Wang, W., Ma, Y., Wang, Y., et al., 2019. Neogene expansion of the Qilian Shan, north Tibet: implications for the dynamic evolution of the Tibetan Plateau. Tectonics 38, 1018–1032. https://doi.org/10.1029/2018TC005258.
Qi, B., Hu, D., Yang, X., Zhang, Y., Tan, C., Zhang, P., Feng, C., 2016. Apatite fission track evidence for the Cretaceous-Cenozoic cooling history of the Qilian Shan (NW China) and for stepwise northeastward growth of the northeastern Tibetan Plateau since early Eocene. J. Asian Earth Sci. 124, 28–41. https://doi.org/10.1016/j.jseaes.2016.04.009.
Qinghai BGMR (Bureau of Geology and Mineral Resources), 1991. Regional Geology of Qinghai Province. Geological Publishing House, Beijing (662 pp.) (in Chinese with English summary).
Rhodes, E.J., 2011. Optically stimulated luminescence dating of sediments over the past 200,000 years. Annu. Rev. Earth Planet. Sci. 39, 461–488. https://doi.org/10.1146/annurev-earth-040610-133425.
Richards, J.P., 2011. Magmatic to hydrothermal metal fluxes in convergent and collided margins. Ore Geol. Rev. 40 (1), 1–26.
Ritts, B.D., Biffi, U., 2000. Magnitude of post-Middle Jurassic (Bajocian) displacement on the central Altyn Tagh fault system, northwest China. Geol. Soc. Am. Bull. 112 (1), 61–74. https://doi.org/10.1130/0016-7606(2000)112<61:MOPJBD>2.0.CO;2.
Ritts, B.D., Yue, Y., Graham, S.A., Sobel, E.R., Abbink, O.A., Stockli, D., 2008. From sea level to high elevation in 15 million years: uplift history of the northern Tibetan Plateau margin in the Altun Shan. Am. J. Sci. 308 (5), 657–678. https://doi.org/10.2475/05.2008.01.
Robinson, D.M., Dupont-Nivet, G., Gehrels, G.E., Zhang, Y., 2003. The Tula uplift, northwestern China: evidence for regional tectonism of the northern Tibetan Plateau during late Mesozoic-early Cenozoic time. Geol. Soc. America Bull. 115, 35–47. https://doi.org/10.1130/0016-7606(2003)115<0035:TTUNCE>2.0.CO;2.
Ryan, W.B., Carbotte, S.M., Coplan, J.O., O'Hara, S., Melkonian, A., Arko, R., Weissel, R.A., Ferrini, V., Goodwillie, A., Nitsche, F., Bonczkowski, J., Zemsky, R., 2009. Global multi-resolution topography synthesis. Geochem. Geophys. Geosyst. 10, Q03014. https://doi.org/10.1029/2008GC002332.
Seeber, L., Gornitz, V., 1983. River profiles along the Himalayan arc as indicators of active tectonics. Tectonophysics 92 (4), 335–367.
Shi, W., Wang, F., Yang, L., Wu, L., Zhang, W., 2018. Diachronous growth of the Altyn Tagh Mountains: constraints on propagation of the northern Tibetan margin from (U-Th)/He dating. J. Geophys. Res. Solid Earth 123, 6000–6018. https://doi.org/10.1029/2017JB014844.
Sobel, E.R., Arnaud, N., 1999. A possible middle Paleozoic suture in the Altyn Tagh, NW China. Tectonics 18 (1), 64–74. https://doi.org/10.1029/1998TC900023.
Sobel, E.R., Arnaud, N., Jolivet, M., Ritts, B.D., Brunei, M., 2001. Jurassic to Cenozoic exhumation history of the Altyn Tagh range, northwest China, constrained by $^{40}Ar/^{39}Ar$ and apatite fission track thermochronology. In: Hendrix, M.S., Davis, G.A. (Eds.), Paleozoic and Mesozoic Tectonic Evolution of Central Asia: From Continental Assembly to Intracontinental Deformation. vol. 194. Geological Society of America, Boulder, CO, pp. 247–267.
Sobel, E.R., Oskin, M., Burbank, D., Miskolaichuk, A., 2006. Exhumation of basementcored uplifts: example of the Kyrgyz range quantified with apatite fission track thermochronology. Tectonics 25, TC2008. https://doi.org/10.1029/2005TC001809.
Spurlin, M.S., Yin, A., Horton, B.K., Zhou, J.Y., Wang, J.H., 2005. Structural evolution of the Yushu-Nangqian region and its relationship to syncollisional igneous activity, east-central Tibet. Geol. Soc. Am. Bull. 117, 1293–1317. https://doi.org/10.1130/B25572.1.
Sun, J., Zhu, R., An, Z., 2005. Tectonic uplift in the northern Tibetan Plateau since 13.7 Ma ago inferred from molasse deposits along the Altyn Tagh Fault. Earth Planet. Sci. Lett. 235 (3–4), 641–653. https://doi.org/10.1016/j.epsl.2005.04.034.
Tapponnier, P., Molnar, P., 1977. Active faulting and tectonics in China. J. Geophys. Res. 82 (20), 2905–2930. https://doi.org/10.1029/JB082i020p02905.
Tapponnier, P., Zhiqin, X., Roger, F., Meyer, B., Arnaud, N., Wittlinger, G., Jingsui, Y., 2001. Oblique stepwise rise and growth of the Tibet Plateau. Science 294 (5547), 1671–1677. https://doi.org/10.1126/science.105978.
Taylor, M., Yin, A., 2009. Active structures of the Himalayan-Tibetan orogen and their relationships to earthquake distribution, contemporary strain field, and Cenozoic volcanism. Geosphere 5 (3), 199–214. https://doi.org/10.1130/GES00217.1.
Van Der Woerd, J., Tapponnier, P.J., Ryerson, F., Meriaux, A.S., Meyer, B., Gaudemer, Y., Finkel, R.C., Caffee, M.W., Zhao, G., Xu, Z., 2002. Uniform postglacial slip-rate along the central 600 km of the Kunlun Fault (Tibet), from ^{26}Al, ^{10}Be, and ^{14}C dating of riser offsets, and climatic origin of the regional morphology. Geophys. J. Int. 148 (3), 356–388.
Vermeesch, P., 2009. RadialPlotter: a Java application for fission track, luminescence and other radial plots. Radiat. Meas. 44, 409–410. https://doi.org/10.1016/j.radmeas.2009.05.003.
Wang, A., Wang, G., Zhang, K., Xiang, S., Li, D., Liu, D., 2009. Late Neogene mountain building of eastern Kunlun orogen: constrained by DEM analysis. J. Earth Sci. 20 (2), 391–400. https://doi.org/10.1007/s12583-009-0032-1.
Wang, E., Xu, F.Y., Zhou, J.X., Wan, J., Burchfiel, B.C., 2006. Eastward migration of the Qaidam basin and its implications for Cenozoic evolution of the Altyn Tagh fault and associated river systems. Geol. Soc. Am. Bull. 118 (3–4), 349–365. https://doi.org/10.1130/b25778.1.
Wang, F., Shi, W., Zhang, W., Wu, L., Yang, L., Wang, Y., Zhu, R., 2017a. Differential growth of the northern Tibetan margin: evidence for oblique stepwise rise of the Tibetan Plateau. Sci. Rep. 7 (1), 41164. https://doi.org/10.1038/srep41164.
Wang, W., Zhang, P., Pang, J., Garzione, C., Zhang, H., Liu, C., et al., 2016a. The Cenozoic growth of the Qilian Shan in the northeastern Tibetan Plateau: a sedimentary archive from the Jiuxi Basin. J. Geophys. Res. Solid Earth 121, 2235–2257. https://doi.org/10.1002/2015JB012689.
Wang, W., Zhang, P., Liu, C., Zheng, D., Yu, J., Zheng, W., et al., 2016b. Pulsed growth of the West Qinling at ~30 Ma in northeastern Tibet: evidence from Lanzhou Basin magnetostratigraphy and provenance. J. Geophys. Res. Solid Earth 121, 7754–7774. https://doi.org/10.1002/2016JB013279.
Wang, W., Zheng, W., Zhang, P., Li, Q., Kirby, E., Yuan, D., et al., 2017b. Expansion of the Tibetan Plateau during the Neogene. Nat. Commun. 8 (1), 15,887. https://doi.org/10.1038/ncomms15887.
Wang, W.T., Zhang, P.Z., Kirby, E., Wang, L.H., Zhang, G.L., Zheng, D.W., Chai, C.Z., 2011. A revised chronology for Tertiary sedimentation in the Sikouzi basin: implications for the tectonic evolution of the northeastern corner of the Tibetan Plateau. Tectonophysics 505 (1–4), 100–114. https://doi.org/10.1016/j.tecto.2011.04.006.
Wang, W., Zheng, D., Li, C., Wang, Y., Zhang, Z., Pang, J., Wang, Y., Yu, J., Wang, Y., Zheng, W., Zhang, H., Zhang, P., 2020. Cenozoic exhumation of the Qilian Shan in the Northeastern Tibetan Plateau: evidence from low-temperature thermochronology. Tectonics 39 (4). https://doi.org/10.1029/2019tc005705. in press.
Wang, X., Wang, B., Qiu, Z., Xie, G., Xie, J., Downs, W., et al., 2003. Danghe area (western Gansu, China) biostratigraphy and implications for depositional history and tectonics of northern Tibetan Plateau. Earth Planet. Sci. Lett. 208 (3–4), 253–269. https://doi.org/10.1016/S0012-821X(03)00047-5.
Wang, Y., Zheng, J., Zheng, Y., 2018. Mesozoic-Cenozoic exhumation history of the Qimen Tagh Range, northeastern margins of the Tibetan Plateau: evidence from apatite fission track analysis. Gondwana Res. 58, 16–26. https://doi.org/10.1016/j.gr.2018.01.014.
Wu, C., Yin, A., Zuza, A.V., Zhang, J.Y., Liu, W.C., Ding, L., 2016. Pre-Cenozoic geologic history of the central and northern Tibetan Plateau and the role of Wilson cycles in constructing the Tethyan orogenic system. Lithosphere 8, 254–292. https://doi.org/10.1130/L494.1.
Wu, C., Zuza, A.V., Chen, X.H., Ding, L., Levy, D.A., Liu, C.F., Liu, W.C., Jiang, T., Stockli, D.F., 2019a. Tectonics of the Eastern Kunlun Range: Cenozoic reactivation of a Paleozoic–early Mesozoic orogen. Tectonics 38 (5), 1609–1650.

Wu, C., Zuza, A.V., Zhou, Z.G., Yin, A., McRivette, M.W., Chen, X.H., Ding, L., Geng, J.Z., 2019b. Mesozoic–Cenozoic evolution of the Eastern Kunlun Range, central Tibet, and implications for basin evolution within the Indo-Asian collision. Lithosphere 11 (4), 524–550. https://doi.org/10.1130/L1065.1.

Wu, C., Liu, C., Fan, S., Zuza, A.V., Ding, L., Liu, W., Ye, B., Yang, S., Zhou, Z., 2020. Structural analysis and tectonic evolution of the western domain of the Eastern Kunlun Range, northwest Tibet. GAS Bull. https://doi.org/10.1130/B35388.1.

Wu, C.L., Gao, Y.H., Lei, M., Qin, H.P., Liu, C.H., Li, M.Z., Frose, B.R., Wooden, J.L., 2014. Zircon SHRIMP U-Pb dating, Lu-Hf isotopic characteristics and petrogenesis of the Paleozoic granites in Mangya area, southern Altun, NW China. Acta Petrol. Sin. 30 (8), 2297–2323 (Yanshi Xuebao). (in Chinese with English abstract).

Wu, L., Xiao, A., Wang, L., Shen, Z., Zhou, S., Chen, Y., Guan, J., 2011. Late Jurassic-early Cretaceous northern Qaidam basin, NW China: implications for the earliest Cretaceous intracontinental tectonism. Cretac. Res. 32 (4), 552–564. https://doi.org/10.1016/j.cretres.2011.04.002.

Wu, L., Lin, X., Cowgill, E., Xiao, A., Cheng, X., Chen, H., et al., 2019. Middle Miocene reorganization of the Altyn Tagh fault system, northern Tibetan Plateau. Geol. Soc. Am. Bull. 131 (7–8), 1157–1178. https://doi.org/10.1130/B31875.1.

Xia, G.Q., Wu, C.H., Li, G.J., Li, G.W., Yi, H.S., Wagreich, M., 2020. Cenozoic growth of the Eastern Kunlun Range (northern Tibetan Plateau): evidence from sedimentary records in the southwest Qaidam Basin. Int. Geol. Rev. https://doi.org/10.1080/00206814.2020.1731717. (in press).

Xinjiang Bureau of Geology and Mineral Resources (BGMR), 1993. Regional Geology of Xinjiang Uygur Autonomous Region: Geological Memoirs of the Ministry of Geology and Mineral Resources. Geological Publishing House, Beijing, P.R. China (841 pp.) (in Chinese with English abstract).

Xinjiang Bureau of Geology and Mineral Resources (BGMR), 2003. Geological Map of Qiemo, Xinjiang, China, Scale 1:25,000: Hubei Autonomous Region Regional Geological Survey Institute. Geological Publishing House, Beijing, P.R. China (350 pp.) (in Chinese).

Yakovlev, P.V., 2015. Evolution of the Indo-Asian Orogen: Insights from the Deformation of the Northern Tibetan Plateau, Mass Balance Calculations, and Volcanic Geochemistry [Ph.D Thesis]. University of Michigan, Ann Arbor, Michigan (296 pp.).

Yan, M., Van der Voo, R., Fang, X., Parés, J.M., Rea, D.K., 2006. Paleomagnetic evidence for a mid-Miocene clockwise rotation of about 25° of the Guide Basin area in NE Tibet. Earth Planet. Sci. Lett. 241 (1–2), 234–247. https://doi.org/10.1016/j.epsl.2005.10.013.

Yang, Z., Li, X., 2006. SHRIMP U-Pb dating of zircons from low-grade metamorphic rocks in the Rola Kangri junction zone, northern Tibet, China. Geol. Bull. China 25, 118–123 (in Chinese with English abstract).

Yin, A., 2010. Cenozoic tectonic evolution of Asia: a preliminary synthesis. Tectonophysics 488, 293–325. https://doi.org/10.1016/j.tecto.2009.06.002.

Yin, A., Harrison, T.M., 2000. Geologic evolution of the Himalayan-Tibetan orogen. Annu. Rev. Earth Planet. Sci. 28, 211–280. https://doi.org/10.1146/annurev.earth.28.1.211.

Yin, A., Rumelhart, P.E., Butler, R., Cowgill, E., Harrison, T.M., Foster, D.A., Ingersoll, R.V., Qing, Z., Xian-Qiang, Z., Xiao-Feng, W., Hanson, A., Raza, A., 2002. Tectonic history of the Altyn Tagh fault system in northern Tibet inferred from Cenozoic sedimentation. Geol. Soc. Am. Bull. 114 (10), 1257–1295. https://doi.org/10.1130/0016-7606(2002)114<1257:THOTAT>2.0.CO;2.

Yin, A., Dang, Y., Zhang, M., McRivette, M.W., Burgess, W.P., Chen, X.H., 2007. Cenozoic tectonic evolution of Qaidam basin and its surrounding regions (Part 2): wedge tectonics in southern Qaidam basin and the Eastern Kunlun Range. In: Sears, J.W. (Ed.), *Whence the Mountains? Inquiries into the Evolution of Orogenic Systems:* A Volume in Honor of Raymond A. Price. vol. 433. Geological Society of America Special Paper, pp. 369–390. https://doi.org/10.1130/2007.2433(18).

Yin, A., Dang, Y.Q., Zhang, M., Chen, X.H., McRivette, M.W., 2008a. Cenozoic tectonic evolution of the Qaidam Basin and its surrounding regions (Part 3): structural geology, sedimentation, and regional tectonic reconstruction. Geol. Soc. Am. Bull. 120 (7–8), 847–876. https://doi.org/10.1130/B26232.1.

Yin, A., Dang, Y.Q., Wang, L.C., Jiang, W.M., Zhou, S.P., Chen, X.H., et al., 2008b. Cenozoic tectonic evolution of Qaidam basin and its surrounding regions (Part 1): the southern Qilian Shan-Nan Shan thrust belt and northern Qaidam basin. Geol. Soc. Am. Bull. 120 (7–8), 813–846. https://doi.org/10.1130/B26180.1.

Yu, J., Zheng, D., Pang, J., Wang, Y., Fox, M., Vermeesch, P., et al., 2019a. Miocene range growth along the Altyn Tagh fault: insights from apatite fission track and (U-Th)/He thermochronometry in the western Danghenan Shan, China. J. Geophys. Res. Solid Earth 124, 9433–9453. https://doi.org/10.1029/2019JB017570.

Yu, J.X., Pang, J.Z., Wang, Y.Z., Zheng, D.W., Liu, C.C., Wang, W.T., et al., 2019b. Mid-Miocene uplift of the northern Qilian Shan as a result of the northward growth of the northern Tibetan Plateau. Geosphere 15 (2), 423–432. https://doi.org/10.1130/GES01520.1.

Yu, X.J., Guo, Z., Chen, Y., Du, W., Wang, Z., Bian, Q., 2020. River system reformed by the Eastern Kunlun Fault: implications from geomorphological features in the Eastern Kunlun Mountains, Northern Tibetan Plateau. Geomorphology 350. https://doi.org/10.1016/j.geomorph.2019.106876.

Yuan, D.Y., Champagnac, J.D., Ge, W.P., Molnar, P., Zhang, P.Z., Zheng, W.J., et al., 2011. Late Quaternary right-lateral slip rates of faults adjacent to the lake Qinghai, northeastern margin of the Tibetan Plateau. Geol. Soc. Am. Bull. 123 (9–10), 2016–2030. https://doi.org/10.1130/B30315.1.

Yuan, D.Y., Ge, W.P., Chen, Z.W., Li, C.Y., Wang, Z.C., Roe, G.H., 2013. The growth of north-eastern Tibet and its relevance to large-scale continental geodynamics: a review of recent studies. Tectonics 32, 1358–1370. https://doi.org/10.1002/tect.20081.

Yuan, W., Dong, J., Shicheng, W., Carter, A., 2006. Apatite fission track evidence for Neogene uplift in the eastern Kunlun Mountains, northern Qinghai-Tibet Plateau, China. J. Asian Earth Sci. 27 (6), 847–856. https://doi.org/10.1016/j.jseaes.2005.09.002.

Yue, Y., Liou, J.G., 1999. Two-stage evolution model for the Altyn Tagh fault, China. Geology 27 (3), 227–230. https://doi.org/10.1130/0091-7613(1999)027<0227:TSEMFT>2.3.CO;2.

Zhang, B.H., Zhang, J., Wang, Y.N., Zhao, H., Li, Y.F., 2017b. Late Mesozoic-Cenozoic exhumation of the Northern Hexi Corridor: constrained by apatite fission track ages of the Longshoushan. Acta Geol. Sin. 91 (5), 1624–1643. https://doi.org/10.1111/1755-6724.13402. (English edition).

Zhang, H., Kirby, E., Pitlick, J., Anderson, R.S., Zhang, P., 2017a. Characterizing the transient geomorphic response to base-level fall in the northeastern Tibetan Plateau. J. Geophys. Res. Earth Surf. 122 (2), 546–572. https://doi.org/10.1002/2015JF003715.

Zhang, J.Y., Liu-Zeng, J., Scherler, D., Yin, A., Li, Z.F., 2018. Spatiotemporal variation of late quaternary river incision rates in southeast tibet, constrained by dating fluvial terraces. Lithosphere 10 (5), 662–675.

Zhang, J., Wang, Y., Zhang, B., Zhao, H., 2015. Evolution of the NE Qinghai-Tibetan Plateau, constrained by the apatite fission track ages of the mountain ranges around the Xining Basin in NW China. J. Asian Earth Sci. 97, 10–23. https://doi.org/10.1016/j.jseaes.2014.10.002.

Zhang, Z.C., Gong, J.Y., Wang, X.F., Guo, Z.J., Zhang, C., 2008. ^{40}Ar-^{39}Ar and fission track analysis of eastern segment of Altyn Tagh fault and its geological significance. Acta Petrol. Sin. 24 (5), 1041–1053 (in Chinese with English abstract).

Zheng, D., Zhang, P.Z., Wan, J., Yuan, D., Li, C., Yin, G., et al., 2006. Rapid exhumation at ~8 Ma on the Liupan Shan thrust fault from apatite fission-track thermochronology: implications for growth of the northeastern Tibetan Plateau margin. Earth Planet. Sci. Lett. 248 (1–2), 198–208. https://doi.org/10.1016/j.epsl.2006.05.023.

Zheng, D., Clark, M.K., Zhang, P., Zheng, W., Farley, K.A., 2010. Erosion, fault initiation and topographic growth of the North Qilian Shan (northern Tibetan Plateau). Geosphere 6 (6), 937–941. https://doi.org/10.1130/GES00523.1.

Zheng, D., Wang, W., Wan, J., Yuan, D., Liu, C., Zheng, W., et al., 2017. Progressive northward growth of the northern Qilian Shan-Hexi Corridor (northeastern Tibet) during the Cenozoic. Lithosphere 9 (3), 408–416. https://doi.org/10.1130/L587.1.

Zhong, J.H., Wen, Z.F., Guo, Z.Q., Wang, H.Q., Gao, J.B., 2004. Paleogene and early Neogene lacustrine reefs in the western Qaidam Basin, China. Acta Geol. Sin. 78, 736–743 (English edition).

Zhuang, G., Hourigan, J.K., Ritts, B.D., Kent-Corson, M.L., 2011. Cenozoic multiple-phase tectonic evolution of the northern Tibetan Plateau: constraints from sedimentary records from Qaidam basin, Hexi Corridor, and Subei basin, northwest China. Am. J. Sci. 311 (2), 116–152. https://doi.org/10.2475/02.2011.02.

Zhuang, G., Johnstone, S.A., Hourigan, J., Ritts, B., Robinson, A., Sobel, E.R., 2018. Understanding the geologic evolution of Northern Tibetan Plateau with multiple thermochronometers. Gondwana Res. 58, 195–210. https://doi.org/10.1016/j.gr.2018.02.014.

Zuza, A.V., Yin, A., 2016. Continental deformation accommodated by non-rigid passive bookshelf faulting: an example from the Cenozoic tectonic development of northern Tibet. Tectonophysics 677–678, 227–240. https://doi.org/10.1016/j.tecto.2016.04.007.

Zuza, A.V., Yin, A., Lin, J., Sun, M., 2017. Spacing and strength of active continental strike-slip faults. Earth Planet. Sci. Lett. 457, 49–62. https://doi.org/10.1016/j.epsl.2016.09.041.

Zuza, A.V., Wu, C., Reith, R.C., Yin, A., Li, J.H., Zhang, J.Y., Zhang, Y.X., Wu, L., Liu, W.C., 2018. Tectonic evolution of the Qilian Shan: an early Paleozoic orogen reactivated in the Cenozoic. Geol. Soc. Am. Bull. 130 (5–6), 881–925. https://doi.org/10.1130/B31721.1.

Zuza, A.V., Wu, C., Wang, Z.Z., Levy, D., Li, B., Xiong, X.S., Chen, X.H., 2019. Underthrusting and duplexing beneath the northern Tibetan Plateau and the evolution of the Himalayan-Tibetan orogen. Lithosphere 11, 209–231. https://doi.org/10.1130/L1042.1.

Zuza, A.V., Thorman, C.H., Henry, C.D., Levy, D.A., Dee, S., Long, S.P., Soignard, E., 2020. Pulsed Mesozoic Deformation in the Cordilleran Hinterland and Evolution of the Nevadaplano: Insights from the Pequop Mountains. NE Nevada, Lithosphere. https://doi.org/10.2113/2020/8850336. (in press).